energies

MDPI

Article

Grid-Connected PV and Battery Energy Storage Systems: A MILP-Based Economic Sensitivity Analysis for the Education Sector

Stefano Mazzoni [1,*], Benedetto Nastasi [1], Ke Yan [2] and Michele Manno [1]

[1] Department of Industrial Engineering, University of Roma Tor Vergata, Via del Politecnico 1, 00133 Rome, Italy; benedetto.nastasi@uniroma2.it (B.N.); michele.manno@uniroma2.it (M.M.)
[2] College of Mechanical and Vehicle Engineering, Hunan University, Changsha, 410082, China; keyan@hnu.edu.cn
* Correspondence: stefano.mazzoni@uniroma2.it

Abstract

This paper develops and applies a techno-economic optimization framework for sizing photovoltaic (PV) and battery energy storage systems (BESSs) in grid-connected energy communities. An in-house developed modeling platform featuring custom MATLAB (R2025a) code implements a mixed-integer linear programming (MILP) model that minimizes differential net present value (NPV) over a 25-year lifetime, integrating capital expenditures, operating cash flows, and carbon taxation. The formulation captures temperature-dependent PV efficiency, battery round-trip efficiency, and time-varying electricity prices, and is validated on a real campus energy community with hourly demand, irradiance, and tariff data. Two design scenarios are examined: the optimal unconstrained case and a budget-constrained configuration (CAPEX $\leq$ 2.0 M€). Results show the unconstrained system installs 3.19 MW_p PV and 12.3 MWh storage, achieving 78.9% self-sufficiency and a 78.9% emissions reduction. The constrained case installs 0.99 MW_p and 1.68 MWh, achieves 32.0% self-sufficiency, and delivers a 4.46 M€ NPV with payback in 3.9 years. Under current costs and tariffs, PV-dominated configurations provide the highest value, with limited battery benefit except under generous budgets or higher carbon prices. A dedicated CAPEX sensitivity analysis explores PV and battery cost variability and its impact on optimal sizing and economic outcomes. The core methodological contribution is a master-planning formulation that solves design decision variables and optimal dispatch concurrently within a single MILP. The flexible platform enables future reassessment as technology, tariff, and policy landscapes evolve.

Keywords: photovoltaic systems; battery energy storage; optimization; net present value; sensitivity analysis; decarbonization

Academic Editor: Antonino S. Aricò

Received: 19 February 2026
Revised: 19 March 2026
Accepted: 28 March 2026
Published: 7 April 2026

1. Introduction

1.1. Background and Motivation

The decarbonization of power systems—accelerated by the Paris Agreement's objectives—is now materially visible in markets: operational PV capacity surpassed 1.6 TW by early 2024 and exceeded 2 TW over 2024, with module prices falling amid strong deployment [1–3]. Updated global cost benchmarks also confirm PV's competitiveness: the levelized cost of electricity (LCOE) for utility-scale PV fell a further 12% between 2022 and 2023, and independent market surveys report continued cost declines [4,5]. This sustained

cost reduction reflects decades of learning-curve effects: PV module costs have declined by approximately 20% for each doubling of cumulative capacity, a pattern documented across multiple technology generations [6,7].

Yet PV's time-varying output creates a structural mismatch with typical building loads, particularly in commercial and industrial facilities where evening demand peaks occur after solar generation has substantially declined. Battery energy storage systems (BESSs) mitigate this temporal mismatch by shifting energy from hours of surplus to hours of scarcity and, increasingly, by enabling grid services such as frequency regulation and demand response [8,9]. Empirical and prospective analyses find that storage value rises with variable renewable energy (VRE) penetration and with the price spread across hours; projected levelized cost of storage (LCOS) trajectories suggest continued cost declines through 2030–2050 [10–12].

At the customer side, the concepts of self-consumption (fraction of PV generation used locally) and self-sufficiency (fraction of load met by local generation) have become key performance indicators, exhibiting distinct behavior and policy sensitivity [13]. In the European Union, the legal framework explicitly recognizes active customers and self-consumption rights through Directive 2019/944, creating regulatory clarity for distributed energy resource investments [14]. Carbon pricing mechanisms—now covering approximately one-quarter of global greenhouse gas emissions—strengthen the private economics of renewable investments, particularly in regions where grid carbon intensity remains elevated [15,16].

1.2. Literature Review

Early PV-BESS sizing methods often relied on heuristic rules or single-objective cost minimization with simplified battery representations. The field has matured toward mixed-integer linear programming (MILP) formulations that co-optimize investment decisions and hourly operational dispatch under realistic tariff structures and technical constraints [17,18]. More recent contributions have extended these formulations with richer techno-economic representations and multi-objective perspectives to explore design trade-offs across building and community contexts [19,20]. These optimization frameworks enable systematic exploration of the design space while guaranteeing global optimality, a critical advantage over heuristic or metaheuristic approaches that may converge to local optima.

Several alternative methodologies have been applied to the PV-BESS sizing and dispatch problem. Heuristic and rule-based strategies—such as threshold-based self-consumption rules or peak-shaving logic—are computationally inexpensive and easy to implement, but they cannot guarantee optimality and may miss non-trivial design interactions between component sizes and operational schedules. Metaheuristic algorithms, including genetic algorithms (GAs), particle swarm optimization (PSO), and simulated annealing, can handle nonlinear and non-convex formulations but offer no formal optimality guarantee, may require extensive parameter tuning, and exhibit sensitivity to initialization [21,22]. Dynamic programming (DP) provides globally optimal solutions for sequential decision problems but faces the "curse of dimensionality" when the state space grows with multiple sizing and dispatch variables [23]. In contrast, MILP formulations exploit the predominantly linear structure of energy balance and economic models, guarantee global optimality via branch-and-bound algorithms, and scale efficiently for the problem sizes typical of community-level design–dispatch co-optimization (thousands of hourly time steps, multiple integer and continuous variables). This combination of optimality assurance and computational tractability motivates the MILP approach adopted in this work.

The economics of energy storage have been extensively analyzed in foundational studies that quantify both energy arbitrage value and ancillary service revenues. Denholm et al. established that storage value increases with VRE penetration as price volatility and curtailment risk rise [9]. The NREL Storage Futures Study synthesized evidence on storage deployment pathways, technology cost projections, and value streams across multiple scenarios [8]. Forward-looking levelized cost of storage analyses project significant cost declines across lithium-ion and alternative technologies by 2030–2050, with lithium-ion LCOS potentially reaching 0.05–0.10 €/kWh for 4 h systems [10,11]. Recent work examining storage durations beyond four hours identifies conditions under which longer-duration technologies become economically competitive as solar penetration increases [12,24].

For customer-sited photovoltaic systems, Luthander et al. provide a comprehensive review of self-consumption drivers, load-generation matching, and policy interactions [13]. Their synthesis identifies technology costs, tariff structures (particularly feed-in versus net-metering policies), and building load profiles as primary determinants of optimal system configurations. On PV performance modeling, the Sandia Array Performance Model and the Faiman temperature model remain widely adopted references in both commercial software (e.g., PVsyst and SAM) [19,25,26] and research applications. Recent comparisons of cell-temperature models highlight the influence of wind speed on temperature predictions and PV performance estimates [25,27]. These models enable accurate prediction of temperature-dependent efficiency losses that can reduce power output by 10–20% during hot summer afternoons compared to standard test conditions.

Technology cost trajectories and learning curves have been extensively documented across energy technologies. Empirical cost datasets and market surveys track rapid cost declines for PV and storage [4,5], while meta-analyses report learning rates of 10–30% across electricity supply technologies, with PV and batteries at the upper end of this range [6,7]. Carbon pricing levels and coverage provide the policy context for internalizing environmental externalities in private project assessments [15,16]. Recommended carbon-price ranges consistent with Paris Agreement temperature goals are summarized by the High-Level Commission on Carbon Prices [15,16], which established that carbon prices of 40–80 USD/tCO_2 by 2020 and 50–100 USD/tCO_2 by 2030 would be consistent with these targets.

Despite this extensive literature, comprehensive multi-dimensional sensitivity analyses that systematically explore interactions among technology costs, carbon pricing, and optimal system configurations remain limited. Most studies vary one or two parameters while holding others constant, potentially missing critical interaction effects where the influence of one parameter depends on the values of others. Furthermore, the rapid pace of cost reductions necessitates periodic reassessment with updated cost structures and market conditions.

In addition, to position the contribution more explicitly, the authors analyze recent works on the joint design–operation optimization of energy communities. Integrated design–operation co-optimization formulations have been proposed by Dal Cin et al. [28] and Carraro et al. [29], while complementary energy-community design optimization studies have addressed different technical and regulatory settings [30,31]. Within the *Energies* literature specifically, several contributions inform the present work: Talluri et al. [32] developed a MILP-based battery scheduling strategy within renewable energy communities, demonstrating significant revenue improvements for prosumers through optimized self-consumption; Simoiu et al. [33] proposed a joint sizing and control methodology for PV–storage systems at district level, explicitly targeting collective self-sufficiency; Ciocia et al. [34] analyzed the interplay between grid injection limits and storage sizing on self-consumption and investment viability for residential PV–battery systems;

Terrier et al. [35] applied a grid-aware MILP to evaluate investment coordination in energy communities from local to national scale, showing that uncoordinated PV deployment can increase costs by up to 83%; and De Souza et al. [36] formulated a multi-objective MILP for energy community design–operation co-optimization, achieving approximately 24% CO_2 reduction with marginal cost increase.

This analysis is structured along three dimensions: (i) the coupling between sizing and dispatch (sequential versus integrated), (ii) the economic perspective (annual operating cost versus lifecycle financial metrics), and (iii) the scope of sensitivity analysis (single-factor checks versus systematic CAPEX mapping). Despite the growing body of work cited above, the analysis highlights that there is still limited evidence on capital-budget-constrained sizing studies that (a) report lifecycle financial metrics (e.g., NPV and payback) under realistic tariff asymmetries and carbon-pricing signals and (b) provide systematic PV–BESS CAPEX sensitivity maps that reveal cost thresholds and technology trade-offs under consistent optimal dispatch. The framework proposed here addresses this gap by coupling investment and hourly operation within a single MILP and by generating PV/BESS CAPEX break-even surfaces for a real educational energy community case study.

1.3. Objectives and Contribution

This paper addresses these gaps through the following contributions:

1. Development and transparent documentation of a mixed-integer linear programming (MILP) model for joint PV-BESS sizing and hourly operational dispatch over a 25-year horizon, implemented in a proprietary MATLAB-based platform, with concurrent optimization of design variables and dispatch to support master-planning decisions.
2. Explicit research-gap analysis of design–operation co-optimization studies for energy communities, motivating the need for budget-constrained lifecycle evaluation and systematic PV–BESS CAPEX mapping under consistent optimal dispatch.
3. Comparative analysis of two design scenarios: an economically optimal unconstrained configuration and a budget-constrained case with 2.0 M€ capital expenditure limit.
4. Complete determination of optimal system capacities (PV and battery), operational dispatch profiles, and grid interaction patterns for both scenarios using integrated techno-economic optimization.
5. Quantification of energy performance metrics (self-sufficiency, self-consumption), economic indicators (NPV, payback period, capital efficiency), and environmental impacts (Scope 2 CO_2 emissions reduction).
6. CAPEX sensitivity analysis across PV and battery cost ranges, mapping break-even regions and cost-driven shifts in optimal sizing and economic performance.
7. Identification of design trade-offs between capital investment, energy autonomy, and economic returns, with implications for energy community planning under diverse financial constraints and policy frameworks.

The remainder of this paper is organized as follows: Section 2 presents the optimization methodology and mathematical formulation; Section 3 describes the case study parameters and sensitivity analysis design with emphasis on the integrated master-planning setup and co-optimized dispatch; Section 4 discusses comprehensive results including detailed contour analysis; and Section 5 provides conclusions and policy implications.

2. Methodology

2.1. System Description and Notation

The system under study is a grid-connected facility integrating photovoltaic generation, battery energy storage, and a bidirectional grid connection. Time is indexed hourly over one representative year $\mathcal{T}$ comprising 8760 time steps, with uniform time step

$\Delta t = 1$ h. The system architecture enables coordinated operation of all components to minimize lifecycle costs while meeting electrical load requirements.

The optimization problem involves the following decision variables:

$n_{\text{PV}} \in \mathbb{Z}_{\geq 0}$	number of PV modules (integer);
$E_{\text{batt,size}}$ [kWh]	nominal battery energy capacity;
$P^{+}_{g,t}, P^{-}_{g,t}$ [kW]	grid import and export power at time t;
$P^{\text{ch}}_{t}, P^{\text{dch}}_{t}$ [kW]	battery charge and discharge power;
E_t [kWh]	battery state of charge (SoC);
P^{PV}_{t} [kW]	PV AC power output;
P^{curt}_{t} [kW]	PV curtailment (if any);
$u^{\text{ch}}_{t}, u^{\text{dch}}_{t} \in \{0, 1\}$	binary variables for charge/discharge logic.

This formulation explicitly represents both sizing decisions (investment variables n_{PV} and $E_{\text{batt,size}}$) and hourly operational decisions (dispatch variables indexed by t), enabling simultaneous optimization of system configuration and operation. This integrated structure targets master-planning problems by co-optimizing design variables and hourly dispatch within a single MILP, so capacity choices are selected alongside their optimal operating trajectories rather than in a sequential planning-then-dispatch workflow. In practice, the optimizer searches over the discrete sizing space while enforcing the hourly operational feasibility constraints and objective within the same problem, delivering a one-stop optimal design-and-dispatch solution. The optimization is performed using realistic time-series data for direct normal irradiance (DNI), ambient temperature, electrical load, and electricity price, as visualized in Figure 1.

Specifically, the DNI data range from 0 to 1000 W/m^2, capturing daily and seasonal variability driven by clear-sky and overcast conditions. Ambient temperature fluctuates between approximately -0.9 and 31.7 °C, directly influencing both PV conversion efficiency and battery performance. The electrical load profile ($P_{\text{el,D}}$) spans 220–1400 kWe, displaying a pronounced daytime peak typical of commercial and light-industrial facilities with sustained operational hours. Electricity price signals ($Price = p^{+}_{t}$) vary between 0.25 and 0.30 €/kWh, reflecting realistic time-of-use differentiation that encourages self-consumption during high-tariff periods. These four input profiles—irradiance, temperature, load, and price—are shown in the vertical subplots of Figure 1, providing the time-series foundations for both the sizing and dispatch optimization models. The electrical load profile used in the model is obtained as:

$$P_{\text{load},t} = P_{\text{el,base},t} + \frac{\dot{Q}_{\text{cool},t}}{\text{COP}_{\text{cool}}} + \frac{\dot{Q}_{\text{heat},t}}{\eta_{\text{heat}}} - P_{\text{DR},t} \tag{1}$$

where $P_{\text{el,base},t}$ is the base electrical demand (lighting, appliances, and other non-thermal electricity uses). The thermal demands for space cooling and heating are assumed to be fully electrified: $\dot{Q}_{\text{cool},t}$ is the cooling thermal power supplied by electric chillers, whose electrical consumption is obtained by dividing by the coefficient of performance COP_{cool}, while $\dot{Q}_{\text{heat},t}$ is the heating thermal power delivered by electric boilers (or heat pumps), whose electrical consumption is obtained by dividing by the conversion efficiency η_{heat}. In this way, the total electrical load $P_{\text{load},t}$ accounts for the electricity drawn by all end-uses, including the electrified thermal services. The term $P_{\text{DR},t}$ represents demand response (load reduction or shifting); it can be incorporated through flexible load variables and constraints, but it is set to zero in this study to keep the focus on the core master-planning formulation. The dot notation emphasizes that $\dot{Q}_{\text{cool},t}$ and $\dot{Q}_{\text{heat},t}$ are thermal power terms

(kW_{th}); with $\Delta t = 1$ h, the corresponding hourly thermal energies are $Q_{cool,t} = \dot{Q}_{cool,t}\Delta t$ and $Q_{heat,t} = \dot{Q}_{heat,t}\Delta t$. In Equation (1), $P_{DR,t} \geq 0$ denotes a downward demand–response reduction (hence the minus sign).

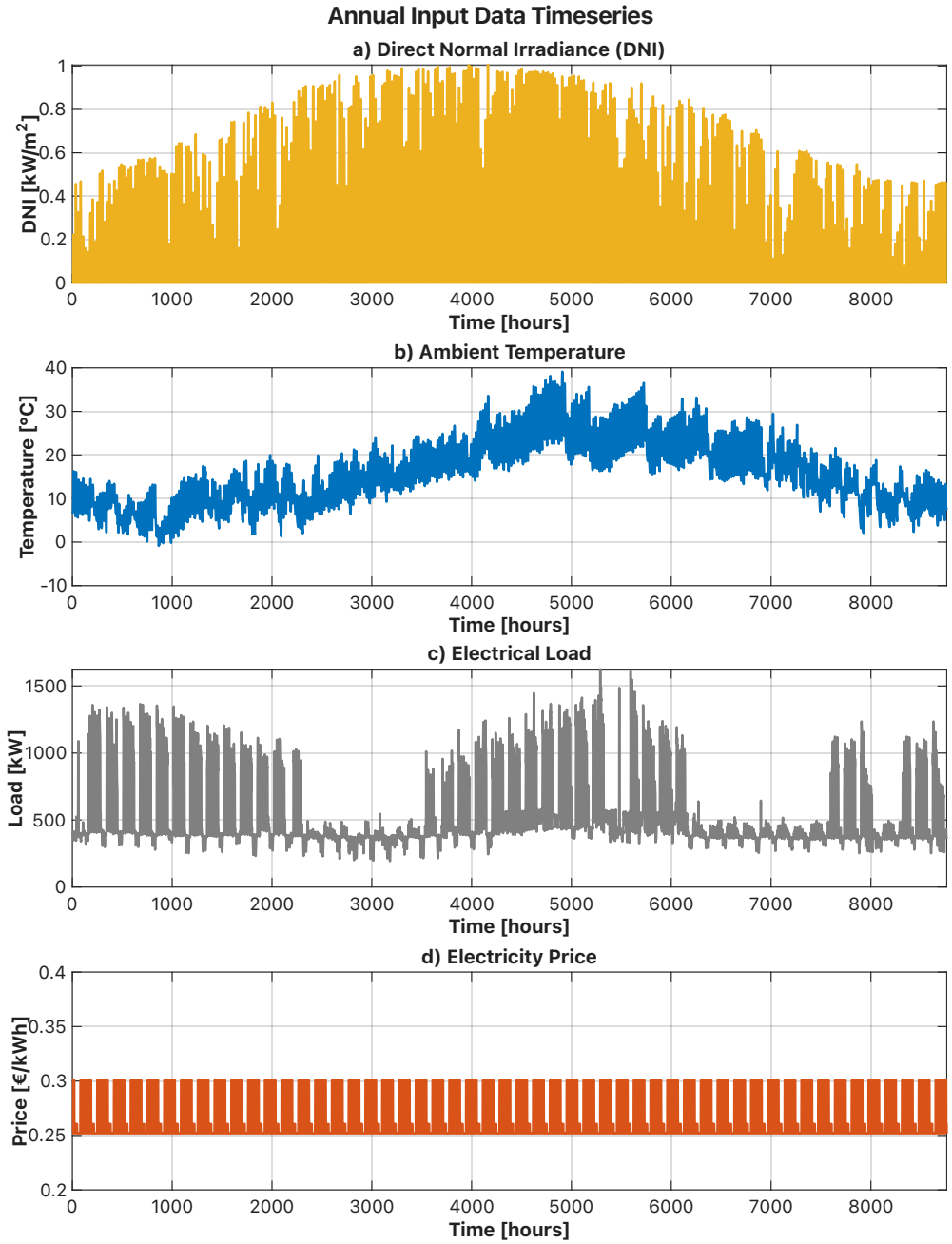

Figure 1. Time-series inputs used in the optimization framework: (**a**) direct normal irradiance (DNI), (**b**) ambient temperature, (**c**) electrical load profile, and (**d**) electricity price signal. These datasets, each spanning one representative meteorological year (8760 h), constitute the exogenous inputs driving both the sizing and dispatch optimization.

Figure 2 summarizes the energy flows considered in the MILP formulation. PV generation (P_{PV}), battery charge/discharge (P_t^{ch}/P_t^{dch}), and grid import/export ($P_{g,t}^{+}/P_{g,t}^{-}$) are balanced at the electrical bus to serve the end-user demand $P_{load,t}$, which is evaluated using Equation (1) and the notation in Table 1.

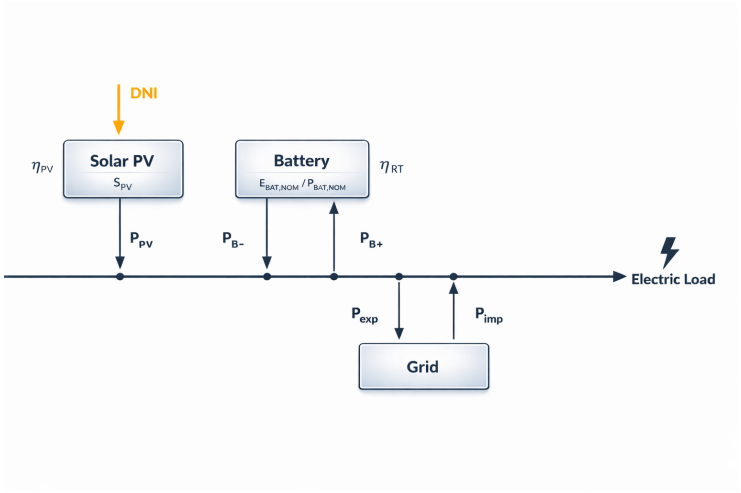

Figure 2. Grid-connect PV and BESS energy system scheme.

Table 1. Summary of modeling assumptions and parameter values.

Category	Parameter	Value
PV system		
	Module efficiency at STC $\eta_{PV,STC}$	0.20
	Reference irradiance G_{STC}	1000 W/m^2
	Reference cell temperature T_{STC}	25 °C
	Solar PV surface S_{unit}	3.3 m^2/panel
	Nominal operating cell temperature NOCT	45 °C
	Specific investment cost C_{PV}	1000 €/kWp
Battery energy storage		
	Round-trip efficiency η_{rt}	0.90
	Specific investment cost C_{batt}	420 €/kWh
	C-rate C_{rate}	1
	Operating SoC band $[E_{min}, E_{max}]$	10–90% of capacity
	Initial/terminal SoC	Periodic: $E_0 = E_{\lvert\mathcal{T}\rvert}$
	Maximum capacity CAP_{batt}^{max}	20,000 MWh
Grid connection and tariffs		
	Maximum import power $P_{g,imp}^{max}$	1000 kW
	Maximum export power $P_{g,exp}^{max}$	1000 kW
	Electricity purchase price range p_t^+	0.25–0.30 €/kWh
	Export price p_t^-	0.5 p_t^+
Emissions and financial parameters		
	Grid carbon intensity $f_{CO_2,grid}$	0.280 kgCO_2/kWh
	Carbon tax τ_{CO_2}	0.10 €/kgCO_2
	Discount rate i_{disc}	0.06
	Maximum CAPEX (constrained) $CAPEX_{max}$	2,000,000 €
	Maximum CAPEX (sensitivity) $CAPEX_{max,sens}$	10,000,000 €
	Fixed capital cost $CAPEX_{fixed}$	300,000 €

2.2. Algorithmic Flow Chart

Figure 3 summarizes the one-stop optimization workflow implemented in MATLAB. The sizing variables and hourly operational decisions are solved concurrently within a single MILP, so capacity choices are selected alongside their optimal dispatch trajectories. The algorithm follows a clear sequence: input time-series data are loaded and checked, system parameters are set, decision variables are declared, and part-load performance parameters (PV efficiency, η_{rt}, and self-discharge σ) are computed. The model then en-

forces time-dependent constraints (power balance and SoC) alongside static bounds and $CAPEX_{max}$, maximizes ΔNPV, and extracts optimal sizing and dispatch results. From a methodological standpoint, the framework treats weather, location, load demand, and price profiles as exogenous time-series inputs. As a result, the same MILP structure can be directly reused for alternative locations or future trajectories by supplying scenario-consistent datasets (e.g., climate-adjusted irradiance and temperature, demand growth and electrification pathways, or evolving tariff structures), and it can be embedded in stochastic or multi-scenario analyses without altering the optimization core. Given that these drivers enter the model purely as data, the sensitivity analysis presented next focuses on tangible investment and policy levers—namely PV/BESS CAPEX and the CO_2-related term—to quantify cost-driven shifts in optimal sizing and economics.

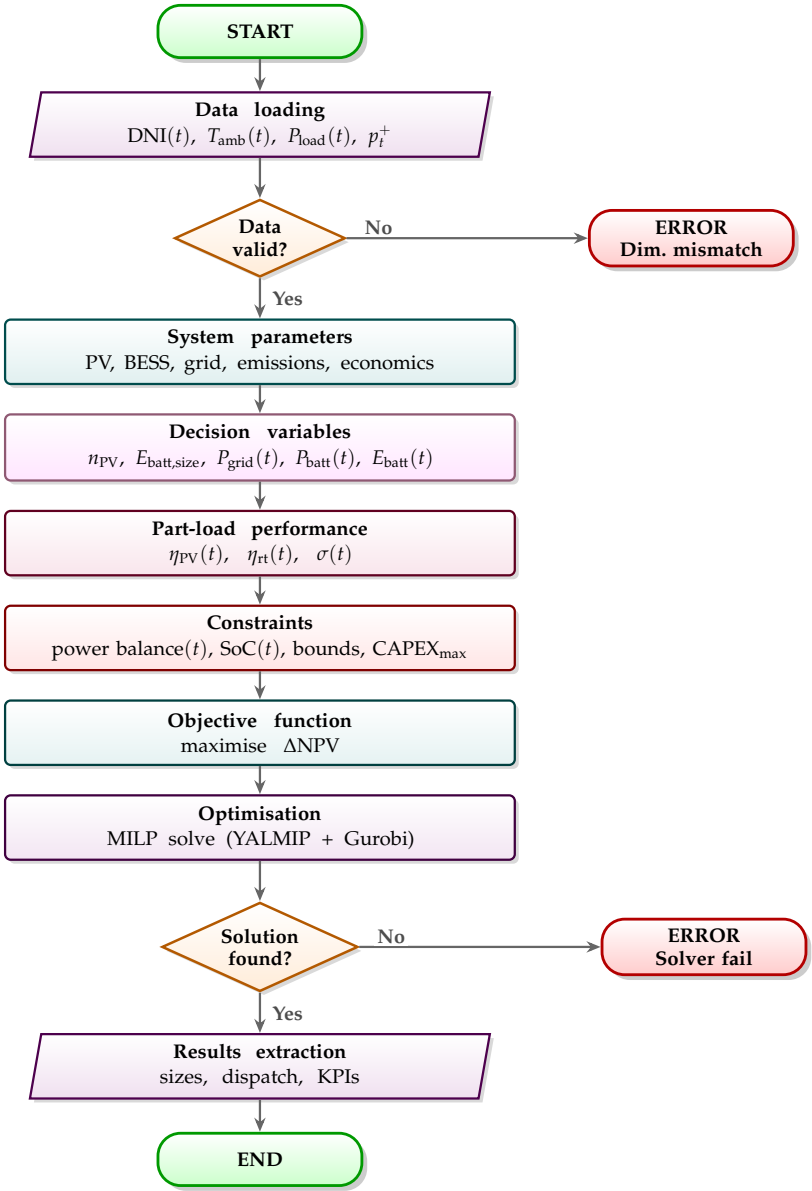

Figure 3. Algorithmic flow chart of the integrated master-planning and dispatch optimization.

2.3. Photovoltaic Generation Model with Temperature Effects

For fixed-tilt arrays, the solar resource available to the modules is characterized by the plane-of-array (POA) irradiance $G_{POA,t}$ [W/m^2], which includes both the direct-beam

and diffuse components after geometric transposition from global horizontal irradiance data [25,27]. The AC power output of the PV array at each time step is then computed as:

$$P_t^{\mathrm{PV}} = n_{\mathrm{PV}}\, S_{\mathrm{unit}}\, \eta_{\mathrm{PV}}(T_{\mathrm{cell},t})\; G_{\mathrm{POA},t}\; \eta_{\mathrm{bos}}\,, \tag{2}$$

where n_{PV} is the number of PV modules (integer decision variable), S_{unit} [m^2] is the aperture area of a single module, $\eta_{\mathrm{PV}}(T_{\mathrm{cell},t})$ [–] is the temperature-dependent DC conversion efficiency (detailed below), and η_{bos} [–] is a lumped balance-of-system efficiency that accounts for inverter conversion, wiring losses, module mismatch, and soiling. The product $n_{\mathrm{PV}} \cdot S_{\mathrm{unit}}$ gives the total array area, which, multiplied by the actual irradiance and efficiencies, yields the net AC power delivered to the electrical bus. When detailed inverter efficiency curves are available, η_{bos} should be modeled as load-dependent; for this analysis, a constant representative value is assumed.

The temperature-dependent module efficiency incorporates the well-established linear temperature coefficient:

$$\eta_{\mathrm{PV}}(T_{\mathrm{cell},t}) = \eta_{\mathrm{STC}}\left[1 + \beta_{\mathrm{temp}}\left(T_{\mathrm{cell},t} - T_{\mathrm{STC}}\right)\right], \tag{3}$$

where η_{STC} is the module efficiency at standard test conditions (25 °C, 1000 W/m^2) and β_{temp} is the temperature coefficient, typically around $-0.45\%/°\mathrm{C}$ for crystalline silicon technology.

Cell temperature $T_{\mathrm{cell},t}$ is estimated using the widely adopted Faiman thermal model [26,27]:

$$T_{\mathrm{cell},t} = T_{\mathrm{amb},t} + \frac{G_{\mathrm{POA},t}}{U_0 + U_1\, v_{\mathrm{wind},t}}, \tag{4}$$

where $T_{\mathrm{amb},t}$ is ambient temperature, $v_{\mathrm{wind},t}$ is wind speed, and (U_0, U_1) are empirically calibrated heat transfer coefficients dependent on mounting configuration (roof-mounted, ground-mounted, building-integrated). When wind speed data are unavailable, the simpler NOCT-based relation provides an acceptable approximation, though it lacks the wind-cooling dependency that can materially affect performance in windy environments.

The installed PV capacity in peak kilowatts is:

$$\mathrm{CAP}_{\mathrm{PV}} = n_{\mathrm{PV}}\, S_{\mathrm{unit}}\, \eta_{\mathrm{STC}}\, \frac{G_{\mathrm{STC}}}{1000}. \tag{5}$$

2.4. Battery Model and Linear Complementarity Constraints

The battery state of charge evolves according to the standard energy balance equation accounting for charge and discharge efficiencies:

$$E_{t+1} = (1-\sigma)E_t + \Delta t\left(\eta_{\mathrm{ch}} P_t^{\mathrm{ch}} - \frac{P_t^{\mathrm{dch}}}{\eta_{\mathrm{dch}}}\right), \tag{6}$$

A self-discharge term can be included in the SoC balance (with σ as the hourly self-discharge rate); in this study, it is set to zero because continuous daily cycling renders self-discharge negligible at the hourly time step.

Where the round-trip efficiency is $\eta_{\mathrm{rt}} = \eta_{\mathrm{ch}}\eta_{\mathrm{dch}}$. For lithium-ion systems, round-trip efficiencies of 85–92% are typical, with our baseline assumption of 90% representing current commercial performance [10,11].

Operational constraints enforce state-of-charge limits and power rating constraints based on C-rate:

$$E_{\min} \leq E_t \leq E_{\max}, \tag{7}$$

$$0 \leq P_t^{\mathrm{ch}} \leq C_{\mathrm{rate}} E_{\mathrm{batt,size}}, \tag{8}$$

$$0 \leq P_t^{\mathrm{dch}} \leq C_{\mathrm{rate}} E_{\mathrm{batt,size}}. \tag{9}$$

The C-rate concept relates power capability to energy capacity: a C-rate of 1.0 h^{-1} indicates the battery can be fully charged or discharged in one hour, implying a power rating equal to energy capacity. Higher C-rates enable more aggressive power cycling but increase power electronics costs.

The SoC band enforces lifetime-preserving limits (here, 10–90% of nominal capacity: $E_{\min} = 0.10\, E_{\mathrm{batt,size}}$, $E_{\max} = 0.90\, E_{\mathrm{batt,size}}$) and a cyclic condition closes the annual simulation:

$$E_0 = E_{|\mathcal{T}|}. \tag{10}$$

This periodic constraint prevents the optimizer from ending the horizon with an artificially depleted or overfilled battery that would overstate economic value.

To prevent simultaneous charge and discharge—a physically meaningless operation that would represent energy recycling through losses—while preserving the linear structure required for MILP solution, the authors introduce binary variables:

$$P_t^{\mathrm{ch}} \leq u_t^{\mathrm{ch}} P_{\max}, \tag{11}$$

$$P_t^{\mathrm{dch}} \leq u_t^{\mathrm{dch}} P_{\max}, \tag{12}$$

$$u_t^{\mathrm{ch}} + u_t^{\mathrm{dch}} \leq 1, \tag{13}$$

where $P_{\max}$ is a sufficiently large constant, tightened in practice to $C_{\mathrm{rate}} E_{\mathrm{batt,size}}$. This formulation is standard in building-scale and distribution-level storage optimization studies [18–20]. Extensions incorporating battery degradation through cycle counting or state-of-health variables can be integrated without fundamentally altering the MILP structure [37,38].

2.5. Grid Connection, Curtailment, and Power Balance

Grid import and export are represented through separate nonnegative variables with independent capacity constraints:

$$0 \leq P_{g,t}^{+} \leq P_{g,\max}^{+}, \qquad 0 \leq P_{g,t}^{-} \leq P_{g,\max}^{-}. \tag{14}$$

Some market rules prohibit simultaneous import and export, which can be enforced through binary variables analogous to the battery logic if required. For most practical applications, economic optimization naturally prevents simultaneous transactions due to price asymmetry (import prices exceed export prices).

The instantaneous power balance constraint enforces nodal equilibrium at each time step:

$$P_t^{\mathrm{PV}} - P_t^{\mathrm{curt}} + P_{g,t}^{+} + P_t^{\mathrm{dch}} = P_{\mathrm{load},t} + P_t^{\mathrm{ch}} + P_{g,t}^{-}, \tag{15}$$

where $P_{\mathrm{load},t}$ is the exogenous electrical load and P_t^{curt} represents voluntary PV curtailment. In practice, economic optimization rarely selects curtailment unless export capacity is constrained or export prices are negative.

2.6. Economic Model and Objective Function

The economic analysis employs time-differentiated electricity prices and carbon taxation to construct hourly cash flows. Let p_t^+ and p_t^- denote import and export electricity prices at time t (€/kWh), reflecting time-of-use tariffs or real-time pricing. Grid carbon intensity f_{CO_2} ($kgCO_2/kWh$) and carbon price τ_{CO_2} (€/$kgCO_2$) determine emission-related costs.

Hourly operational cash flows are:

$$\mathrm{OPEX}(t) = \left(p_t^+ + f_{CO_2}\tau_{CO_2}\right) P_{g,t}^+ \Delta t, \tag{16}$$

$$\mathrm{REV}(t) = \left(p_t^- + f_{CO_2}\tau_{CO_2}\right) P_{g,t}^- \Delta t. \tag{17}$$

The carbon tax credit for exported electricity reflects avoided emissions at the grid margin. Total capital expenditure combines technology-specific costs with fixed installation costs:

$$\mathrm{CAPEX} = \mathrm{CAP}_{\mathrm{PV}} \cdot C_{\mathrm{PV}} + E_{\mathrm{batt,size}} \cdot C_{\mathrm{batt}} + \mathrm{CAPEX}_{\mathrm{fixed}}, \tag{18}$$

where C_{PV} (€/kW_p) and C_{batt} (€/kWh) are PV and battery specific costs, respectively, and $\mathrm{CAPEX}_{\mathrm{fixed}}$ captures non-scalable costs including grid connection upgrades, site preparation, and project development.

The system net present value discounts annual cash flows at rate i_{disc} over project lifetime N_{years}:

$$\mathrm{NPV}_{\mathrm{system}} = -\mathrm{CAPEX} + \sum_{y=1}^{N_{\mathrm{years}}} \frac{\sum_{t\in\mathcal{T}} \left(\mathrm{REV}(t) - \mathrm{OPEX}(t)\right)}{(1+i_{\mathrm{disc}})^y}. \tag{19}$$

The baseline scenario (grid-only counterfactual) establishes the NPV without renewable investment:

$$\mathrm{NPV}_{\mathrm{base}} = -\sum_{y=1}^{N_{\mathrm{years}}} \frac{\sum_{t\in\mathcal{T}} \left(p_t^+ + f_{CO_2}\tau_{CO_2}\right) P_{\mathrm{load},t}\Delta t}{(1+i_{\mathrm{disc}})^y}. \tag{20}$$

The representative meteorological and tariff year is repeated for every project year, so annual cash flows are identical aside from discounting. Tariff escalation or mid-life component replacement can be incorporated by indexing p_t^+, p_t^-, or CAPEX by year when required.

The optimization objective maximizes the differential NPV, which quantifies the economic advantage (or disadvantage) of renewable investment relative to continued grid dependence:

$$\max \quad \Delta\mathrm{NPV} := \mathrm{NPV}_{\mathrm{system}} - \mathrm{NPV}_{\mathrm{base}}. \tag{21}$$

Positive ΔNPV indicates that the renewable system improves economics (higher value than the grid-only baseline). Negative ΔNPV would indicate value destruction relative to the baseline.

Extensions to this economic framework can incorporate salvage value at end-of-life, mid-life component replacement (particularly relevant for batteries with 10–15 year lifetimes), time-varying degradation effects, or demand charge structures common in commercial tariffs [11,19].

2.7. Modeling Assumptions and Scope Limitations

To maintain focus on the core master-planning formulation and ensure computational tractability, the following simplifying assumptions are adopted:

- **No explicit battery degradation:** The SoC band is constrained to 10–90% of nominal capacity, which serves as a proxy for lifetime-preserving operation. Calendar and cycle aging are not modeled explicitly; degradation-aware formulations can be incorporated via piecewise-linear state-of-health constraints without altering the MILP structure [37,38].
- **No PV annual degradation:** Module power output is assumed constant over the 25-year horizon. Typical annual degradation rates of 0.3–0.5%/year for crystalline silicon could be included by applying a year-dependent derating factor to PV generation.
- **No mid-life component replacement:** Battery and inverter replacement costs are not modeled. For lithium-ion systems with 10–15 year lifetimes, a mid-life replacement event could be incorporated by adding a discounted CAPEX term at the replacement year.
- **No explicit O&M costs:** Operations and maintenance expenses are excluded from the objective function; their inclusion would reduce NPV but is unlikely to alter the relative ranking of scenarios under the cost ranges considered.
- **No inter-annual tariff escalation:** Import and export prices follow a time-varying, hourly time-of-use structure within each year (see Figure 1, bottom panel), but the same annual tariff profile is repeated across the 25-year horizon without escalation. This reflects current Italian industrial contracts but does not capture long-term tariff evolution or real-time pricing dynamics.
- **Unconstrained grid connection:** The distribution network is modeled as an unlimited source and sink within the import/export power caps (1 MW each). Network congestion, voltage, and power quality constraints are not represented.

These assumptions are revisited in the concluding section, where the corresponding extensions are identified as future work.

2.8. Performance Metrics

The comparative assessment includes several key performance indicators:

Self-Sufficiency (SS)–Defined as the fraction of total electrical demand satisfied by locally generated renewable energy:

$$SS = \frac{E_{PV,direct} + E_{battery,discharge}}{E_{demand}} \times 100\% \quad (22)$$

Self-Consumption (SC)–Represents the portion of PV generation consumed locally rather than exported to the grid:

$$SC = \frac{E_{\mathrm{PV,direct}} + E_{\mathrm{battery,discharge}}}{E_{\mathrm{PV,total}}} \times 100\% \quad (23)$$

This definition adopts a load-side accounting convention: $E_{\mathrm{battery,discharge}}$ counts only the energy effectively delivered to the demand after round-trip losses, providing a conservative estimate of self-consumption consistent with the convention in Luthander et al. [13]. An alternative generation-side convention that uses battery charge energy ($E_{\mathrm{battery,charge}}$) would yield slightly higher SC values because it credits PV for all energy absorbed locally, including the fraction lost to round-trip inefficiency.

Scope 2 CO_2 Emissions–Quantifies indirect carbon emissions from grid electricity imports using the grid carbon intensity factor:

$$E_{\mathrm{CO_2}} = E_{grid,import} \times f_{\mathrm{CO_2,grid}} \quad (24)$$

where $E_{grid,import}$ is the annual electricity purchased from the grid (kWh) and $f_{CO_2,grid}$ is the grid carbon intensity ($kgCO_2/kWh$).

These metrics provide a comprehensive evaluation framework for assessing the technical, environmental, and economic dimensions of energy community configurations.

3. Case Study and Assumptions

The proposed optimization framework was applied to a representative energy community case study to evaluate the techno-economic feasibility of integrating photovoltaic (PV) systems with battery energy storage systems (BESSs) under different investment scenarios. The analysis focuses on quantifying the trade-offs between capital investment constraints, energy performance metrics, and economic viability, providing insights into optimal sizing strategies for renewable energy communities.

Energy Demand Profile. The case study considers an annual electrical load of 4802.8 MWh, representing a medium-scale energy community with mixed residential and commercial consumption. The load profile exhibits significant temporal variability with peak demands during daytime hours and seasonal variations. Demand data was processed at 1 h resolution for detailed supply–demand matching analysis.

Photovoltaic System Characterization. PV generation potential was evaluated using direct normal irradiance (DNI) and ambient temperature profiles. The temperature-dependent efficiency model accounts for performance degradation through the NOCT formulation, with baseline efficiency $\eta_{PV,STC} = 0.20$ at a reference irradiance of 1000 W/m^2. The specific capital cost was set at 1000 €/kWp, consistent with current market conditions for utility-scale installations. Curtailment was not included in the presented case studies because the analyzed capacity ranges do not lead to structural overproduction relative to community demand and storage capability.

Battery Energy Storage System. The BESS was modeled with round-trip efficiency of 90% ($\eta_{ch} = \eta_{dch} = 0.95$), representative of modern lithium-ion systems. Specific capital cost was 420 €/kWh including cells, BMS, PCS, and installation, plus 300,000 € fixed costs for infrastructure and grid connection. State-of-charge constraints were limited to 10–90% of nominal capacity to preserve battery lifetime.

Grid Interaction and Tariff Structure. The energy community exchanges power bidirectionally with the grid. Electricity purchase price p_t^+ ranges from 0.25 to 0.30 €/kWh following time-varying industrial tariffs, while export price is $p_t^- = 0.5\, p_t^+$, creating strong economic incentives for self-consumption. Grid connection constraints limit maximum import and export power to 1000 kW, representing typical distribution network capacity at medium-voltage connection points.

Economic Parameters and Assessment Methodology. Economic viability was assessed using NPV analysis over a 25-year lifetime with a 6% discount rate, reflecting the weighted average cost of capital for renewable energy infrastructure. Scope 2 carbon emissions were quantified using a grid intensity of 0.280 $kgCO_2/kWh$, with a carbon tax of 100 €/tonne CO_2 incorporated to reflect environmental externalities under European Green Deal objectives.

3.1. Summary of Modeling Assumptions

For transparency and reproducibility, Table 1 summarizes the main numerical assumptions used in the MATLAB implementation of the case study. They correspond directly to the parameter definitions in the simulation script.

3.2. Optimization Scenarios

Two distinct optimization scenarios were formulated to evaluate the impact of capital budget constraints on system design and performance:

Case 1: No Capital Constraint–This scenario represents the economically optimal configuration without any restriction on initial capital expenditure. The optimization algorithm determines PV and BESS capacities that maximize the net present value over the project lifetime, balancing capital costs against operational savings and revenue from energy management. The decision space was intentionally defined with wide bounds so that the economic optimum is not artificially constrained: PV capacity may vary between 0 and 10,000 kWp, while battery energy capacity can range from 0 to 20,000 MWh, subject to the grid, state-of-charge, and investment constraints described above.

Case 2: CAPEX $\leq$ 2.0 M€—This scenario introduces a capital budget constraint representative of typical financing limitations for energy community projects. The total capital expenditure, including both PV and BESS components plus fixed costs, is restricted to a maximum of 2.0 million euros. This constraint forces the optimization to find the best balance between system capacity and economic performance within the available budget, potentially sacrificing some energy autonomy to maintain financial feasibility.

Both scenarios were solved using the Gurobi optimization solver with parallel computation enabled to handle the large-scale mixed-integer linear programming (MILP) formulation. The optimization determines continuous variables for PV and BESS capacities, as well as hourly operational decisions for battery charging/discharging and grid import/export over the entire annual horizon (8760 h). The computational efficiency of the framework is demonstrated by the total solution time of 19 s for both scenarios combined on an Apple M4 Max processor (14-core CPU, 10 neural cores, 36 GB RAM), highlighting the practical applicability of the MILP approach for rapid scenario evaluation and parametric studies in energy community design.

3.3. Sensitivity Analysis Design

The objective of the sensitivity analysis is to quantify how optimal PV and BESS sizing and economic performance respond to plausible variations in technology costs and grid carbon intensity. By mapping regions of cost-competitiveness and break-even behavior, the analysis clarifies the CAPEX-driven trade-offs that shape master-planning decisions.

The results section is structured to highlight the economic impact of CAPEX for the PV and battery technologies under the two investment scenarios.

For the results sections, a fixed grid CO_2 emission factor is assumed, consistent with the baseline $f_{CO_2,\text{grid}}$ reported in Section 3.2.

The three-dimensional sensitivity analysis systematically varies:

- **PV-specific cost** (C_{PV}): [400, 666.7, 933.3, 1200] €/kW$_p$ (4 levels);
- **Battery-specific cost** (C_{batt}): [400, 600, 800, 1000] €/kWh (4 levels);
- **Grid carbon intensity** (f_{CO_2}): [0.260, 0.280, 0.300] kgCO_2/kWh (3 levels).

This design generates $4 \times 4 \times 3 = 48$ distinct scenarios, each requiring a complete mixed-integer optimization over 8760 hourly time steps. For the sensitivity analysis, the investment budget is capped at 10 M€ to avoid unrealistic oversizing while preserving broad exploration of the design space. The parameter ranges encompass current market conditions and plausible near-term cost trajectories based on learning curve projections and industry forecasts [4,5,10].

The MILP formulation is implemented in MATLAB using the YALMIP modeling framework [39] interfaced with the Gurobi commercial optimizer [40]. Parallel execution leverages MATLAB's Parallel Computing Toolbox to distribute scenarios across multiple CPU cores. Each worker executes an independent Gurobi instance, with solver thread

allocation tuned to avoid oversubscription: on a system with N CPU cores and W parallel workers, each Gurobi instance is allocated $\lfloor N/W \rfloor$ threads to maximize throughput while avoiding resource contention. This parallelization strategy achieves 8–12$\times$ computational speedup on modern workstations, reducing total computation time from several hours to 20–40 min depending on hardware specifications.

4. Results and Discussion

The results are organized to facilitate direct comparison between Case 1 (no CAPEX constraint) and Case 2 (CAPEX $\leq$ 2.0 M€). Each subsection first presents the temporal patterns and performance metrics for both scenarios side by side, then draws cross-case insights. A targeted CAPEX sensitivity analysis and a closing discussion of limitations complete the section.

4.1. Case 1 vs. Case 2: Temporal Operation Patterns (Heatmap Comparison)

To provide an intuitive overview of the hourly operation of the energy community, Figures 4 and 5 report heatmaps of demand, PV generation, grid import, grid export, and battery state of charge (SoC) for the two optimization scenarios. Each panel uses the day of the year on the horizontal axis and the hour of day on the vertical axis, allowing persistent patterns and seasonal effects to be visually identified.

The demand heatmaps confirm that the load is strongly concentrated between 08:00 and 18:00 with modest seasonality, whereas PV generation is strictly limited to daylight hours and peaks in the summer months. In Case 1, the large PV and battery capacities result in extended periods with very low grid import and substantial grid export, especially in late spring and summer, as indicated by the dense red and blue bands. The battery SoC panel reveals frequent deep cycling with multi-day storage of energy during periods of high irradiance. In Case 2, by contrast, grid import remains significant throughout the year and grid export almost disappears; the smaller battery cycles over a narrower SoC range that mainly smooths intra-day fluctuations rather than providing multi-day shifting. These patterns visually reinforce the quantitative indicators of self-sufficiency and self-consumption discussed below.

4.2. Optimal System Sizing: Case 1 (Unconstrained) vs. Case 2 (Budget-Constrained)

The optimization results reveal substantial differences between the two scenarios in terms of installed capacities and capital investment requirements. Figure 6 summarizes the optimal PV and battery capacities for both cases, while Figure 7 presents a comprehensive comparison of energy flows, providing insights into the utilization patterns of generation and storage assets. For Case 1 (no capital constraint), the optimization algorithm determined optimal capacities of 3194.4 kWp for PV and 12,312.06 kWh for battery storage (Figure 6), resulting in a total capital expenditure of 8,665,465 €. The breakdown shows 3,194,400 € allocated to the PV system and 5,171,065 € to the battery storage system, with the remaining 300,000 € representing fixed infrastructure costs. This configuration prioritizes energy autonomy and revenue generation from optimized energy arbitrage operations.

The PV generation capacity represents approximately 0.665 kWp per MWh of annual demand, indicating a deliberate oversizing strategy to maximize self-sufficiency and enable significant battery charging during high-irradiance periods. The battery capacity of 12.3 MWh provides substantial temporal shifting capability, representing approximately 2.6 times the average daily demand. This large storage capacity enables the system to buffer multi-day weather variations and optimize grid interaction patterns to minimize costs.

In contrast, Case 2 (CAPEX $\leq$ 2.0 M€) yields a significantly constrained configuration with 993.96 kWp PV capacity and 1680.69 kWh battery storage, totaling 1,999,849 € in capital investment—precisely at the imposed budget limit (Figure 6). The optimization allocated 993,960 € to PV (49.7% of budget) and 705,889 € to batteries (35.3% of budget), with the remaining 300,000 € for fixed costs. This represents a 68.9% reduction in PV capacity and an 86.3% reduction in battery capacity compared to Case 1.

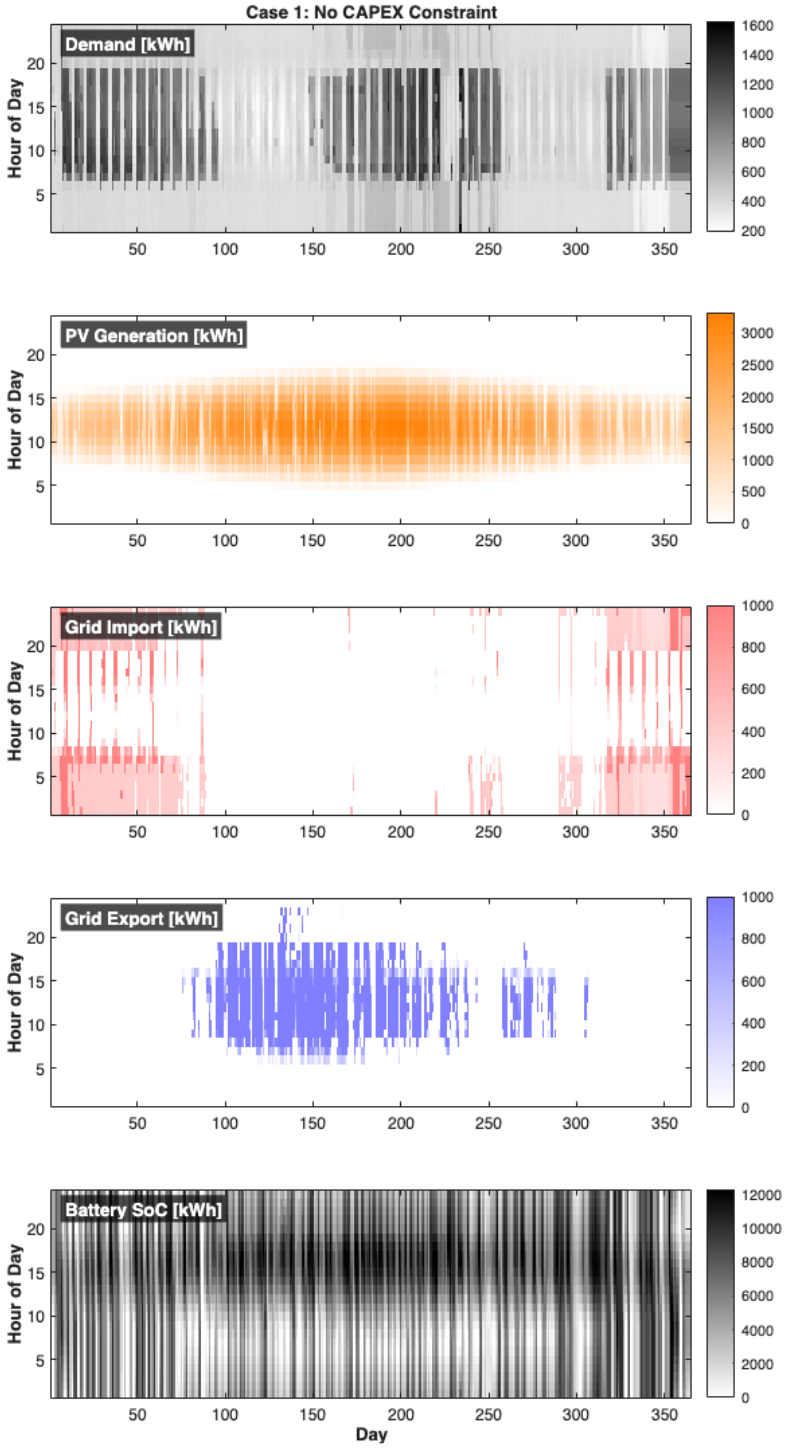

Figure 4. Heatmap dashboard for Case 1 (no CAPEX constraint). From top to bottom: electrical demand, PV generation, grid import, grid export, and battery state of charge (SoC). Each panel uses the day of year on the horizontal axis and the hour of day on the vertical axis; dark bands correspond to periods of sustained high values, while white or pale regions indicate low utilization.

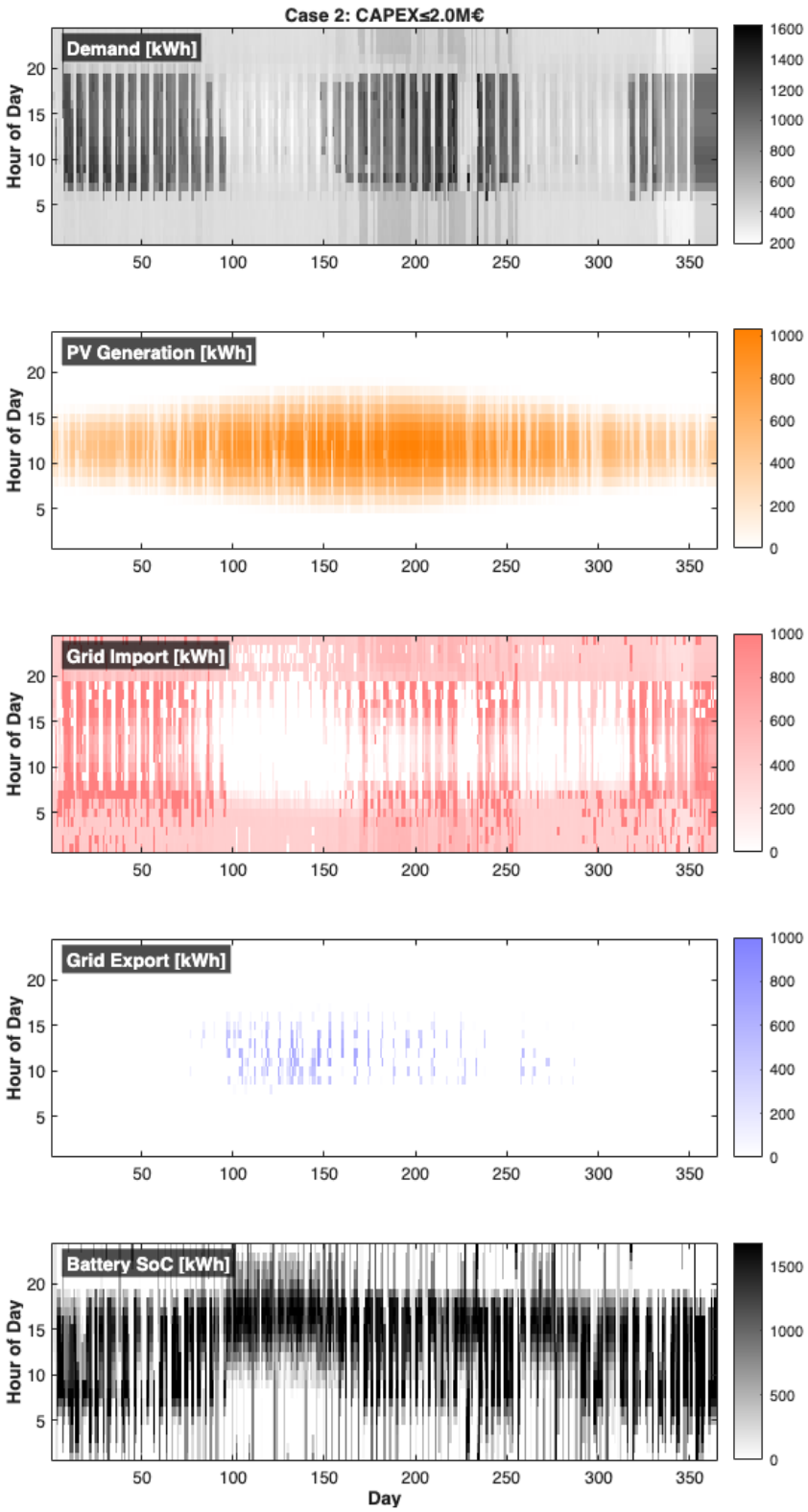

Figure 5. Heatmap dashboard for Case 2 (CAPEX $\leq$ 2.0 M€). The same five variables as in Figure 4 are shown with individually optimized color scales, enabling direct visual comparison of seasonal and diurnal patterns between the two scenarios.

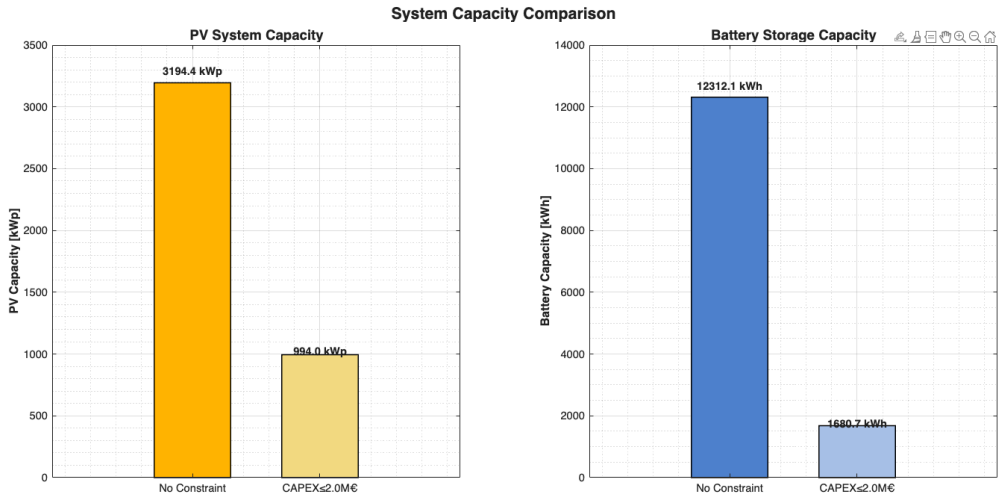

Figure 6. Optimal system capacities obtained from the MILP optimization. Left panel: PV peak power capacity for Case 1 (no CAPEX constraint) and Case 2 (CAPEX $\leq$ 2.0 M€). Right panel: corresponding battery energy capacity. Numerical labels report the exact values in kWp and kWh, highlighting the strong reduction in storage capacity when the investment cap is enforced.

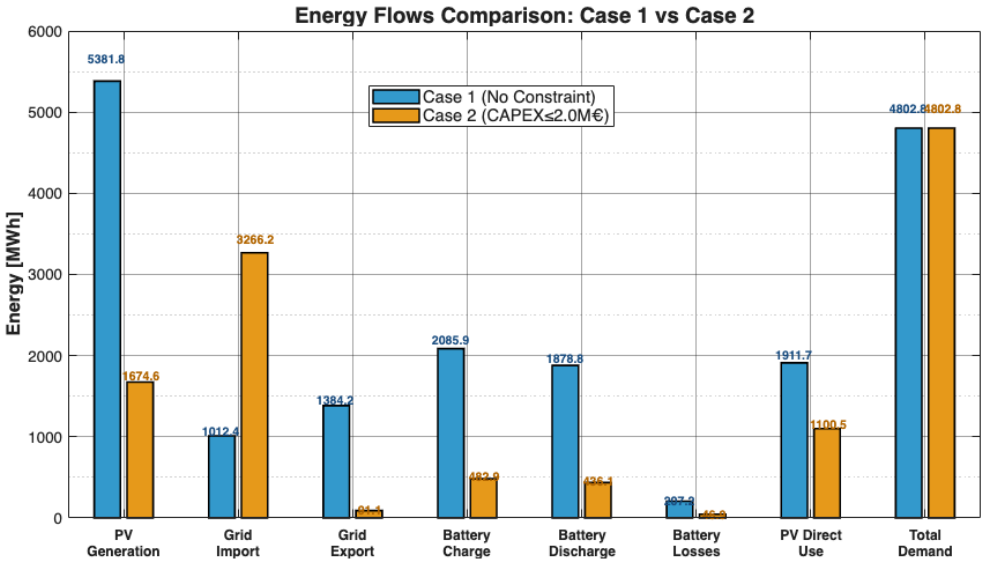

Figure 7. Energy flows comparison between Case 1 (no constraint) and Case 2 (CAPEX $\leq$ 2.0 M€), showing PV generation, grid interaction, battery operation, and total demand.

The dramatic reduction in battery capacity under budget constraints highlights the relatively high specific cost of energy storage compared to generation. The optimization algorithm preferentially allocates limited capital to PV generation, which provides direct energy production, rather than storage, which only provides temporal arbitrage value. This result suggests that for budget-constrained projects, a generation-heavy configuration may be more economically rational than a balanced generation-storage mix.

4.3. Energy Flow Analysis: Case 1 vs. Case 2 Operation

The Sankey diagrams presented in Figure 8 provide detailed visualization of energy pathways through the system, revealing fundamental differences in operational characteristics between the two scenarios.

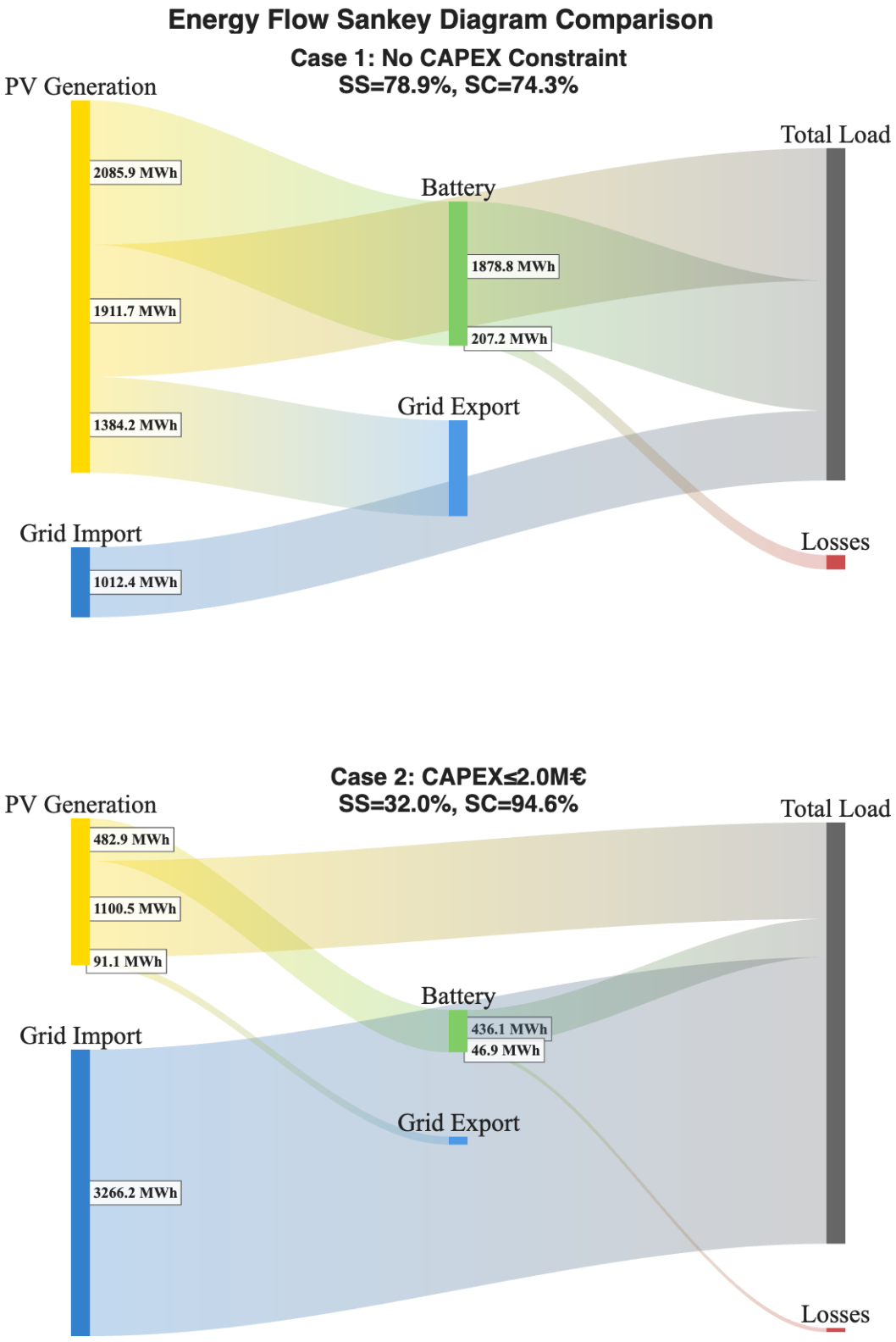

Figure 8. Sankey diagrams illustrating energy flow pathways for Case 1 (**top**) and Case 2 (**bottom**). Yellow flows represent solar energy, blue flows represent grid electricity, green represents battery storage, and red indicates losses. **Important: flow widths are not proportional between diagrams; both cases serve identical total annual demand.**

For Case 1, the total PV generation reaches 5381.8 MWh annually, significantly exceeding the total demand of 4802.8 MWh. This surplus generation is distributed across three pathways: 1911.7 MWh (35.5%) flows directly to the load without storage, 2085.9 MWh

(38.8%) charges the battery for later use, and 1384.2 MWh (25.7%) is exported to the grid. The substantial export component indicates that the system generates excess energy even after maximizing self-consumption and battery charging, creating revenue through feed-in compensation.

The battery subsystem processes 2085.9 MWh of charging energy, of which 1878.8 MWh (90.1%) is successfully discharged to meet load demand, while 207.2 MWh (9.9%) is dissipated as conversion losses.

Grid import remains necessary at 1012.4 MWh (21.1% of total demand), occurring primarily during extended periods of low solar irradiance or when battery state-of-charge reaches minimum limits. The relatively modest import fraction indicates high energy autonomy, with 78.9% of demand met through local renewable generation and storage.

Case 2 exhibits markedly different energy flow characteristics due to reduced system capacities. Annual PV generation drops to 1674.6 MWh, representing only 34.9% of total demand. Of this generation, 1100.5 MWh (65.7%) serves the load directly, 482.9 MWh (28.8%) charges the battery, and only 91.1 MWh (5.4%) is exported to the grid. The minimal export fraction suggests that the system is sized primarily for self-consumption rather than revenue generation.

The smaller battery (1680.69 kWh versus 12,312.06 kWh in Case 1) processes 482.9 MWh charging, with 436.1 MWh discharged and 46.8 MWh lost to inefficiency, maintaining approximately 90.3% round-trip efficiency. However, the reduced storage capacity limits temporal shifting capability, resulting in less effective utilization of PV generation. Grid import increases substantially to 3266.2 MWh (68.0% of demand), more than three times the import level of Case 1, reflecting reduced energy autonomy.

4.4. Self-Sufficiency and Self-Consumption: Case 1 vs. Case 2 Performance

Figure 9 presents monthly and annual self-sufficiency (SS) and self-consumption (SC) metrics, revealing significant seasonal variations and fundamental trade-offs between these complementary indicators.

Case 1 achieves an annual self-sufficiency of 78.9%, meaning that approximately four-fifths of the electrical demand is satisfied through local renewable generation and storage without grid import. Monthly SS values range from 41.8% in January to 100% during peak solar months (April, May, June, July), where the system achieves complete energy autonomy. The summer period (June–August) demonstrates sustained 100% or near-100% self-sufficiency, enabled by high solar irradiance and large battery capacity for overnight storage.

Winter months exhibit reduced SS due to lower solar angles, shorter days, and increased cloud cover. January shows the minimum SS of 41.8%, requiring 58.2% grid import to meet demand. The transition months (March, September, October) show intermediate performance around 60–85%, reflecting seasonal variations in solar resource availability. The annual average of 78.9% represents a favorable balance between renewable energy penetration and system cost.

The self-consumption metric for Case 1 reaches 74.3% annually, indicating that approximately three-quarters of generated PV energy is utilized locally (either directly or via battery storage), while one-quarter is exported to the grid. Monthly SC values exhibit an inverse relationship with SS—winter months achieve higher SC (up to 100% in January and December) because limited generation is fully consumed locally, while summer months show lower SC (54.2% in May) due to substantial surplus generation exceeding local demand and storage capacity.

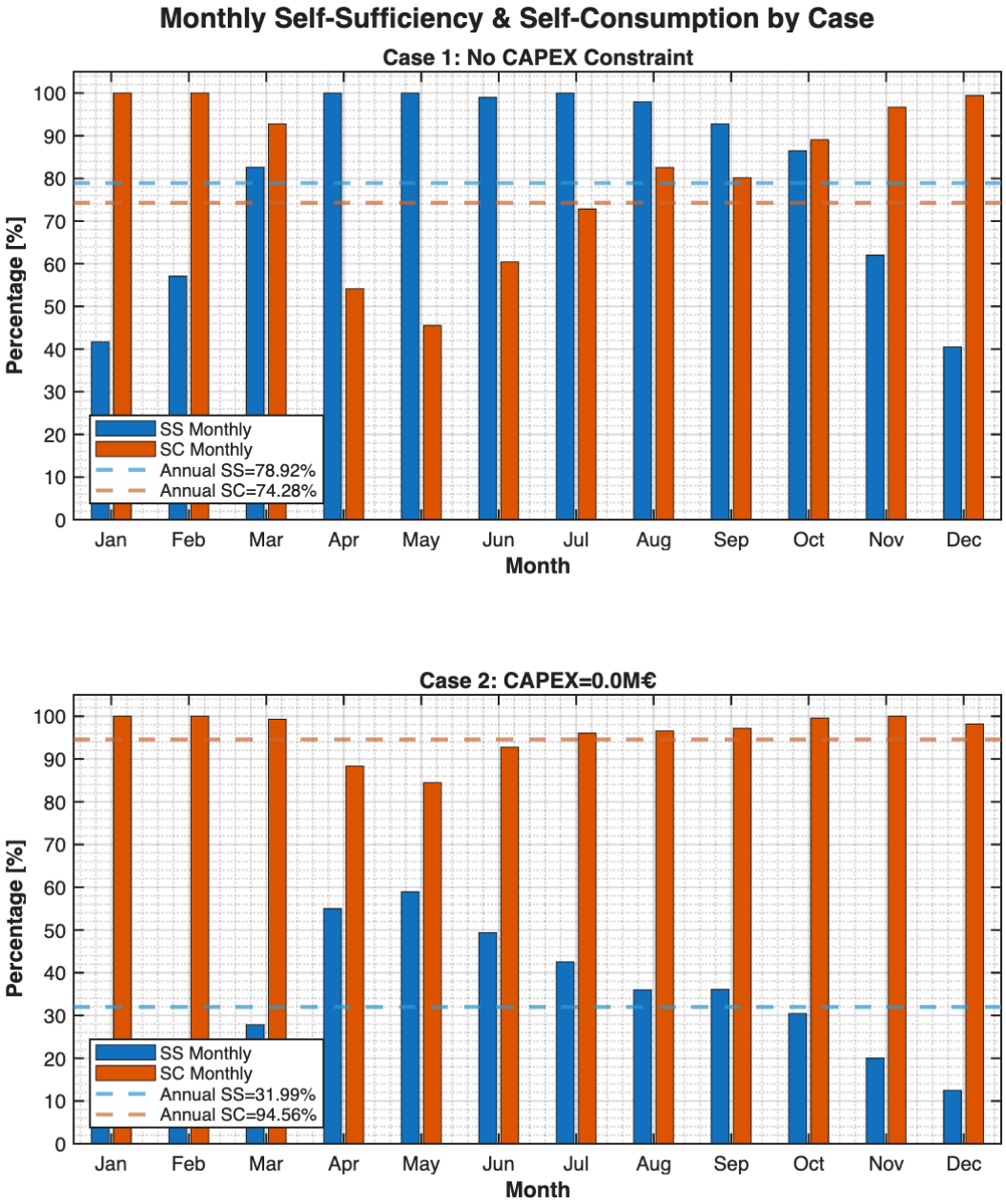

Figure 9. Monthly self-sufficiency (SS) and self-consumption (SC) percentages for Case 1 (**top**) and Case 2 (**bottom**), with dashed lines indicating annual averages.

This inverse correlation between SS and SC represents a fundamental characteristic of oversized renewable systems: high generation capacity improves self-sufficiency but creates excess production that reduces self-consumption ratios. The large battery capacity (12.3 MWh) helps mitigate this effect by storing surplus daytime generation for evening consumption, but cannot fully absorb peak summer production, necessitating grid export.

Case 2 presents contrasting performance characteristics driven by the budget-constrained configuration. Annual self-sufficiency drops to 32.0%—less than half the Case 1 value—reflecting the 68.9% reduction in PV capacity. Monthly SS ranges from 12.8% in January to 59.5% in April, never achieving complete energy autonomy even during peak solar months. The system remains heavily grid-dependent throughout the year, with 68.0% of annual demand requiring grid import.

Conversely, self-consumption improves to 94.6% annually, with monthly values between 84.5% (April) and 100% (January, November, December). This high SC indicates that virtually all generated PV energy is consumed locally, with minimal grid export (only

91.1 MWh annually, or 5.4% of generation). The smaller battery capacity (1680.69 kWh) is appropriately sized to buffer daily generation-demand mismatches without creating excess storage capacity.

The Case 2 configuration represents a right-sized self-consumption optimized system that maximizes utilization of installed assets while accepting lower energy autonomy. This approach aligns with economic rationality under capital constraints: rather than oversizing generation and storage to maximize SS at high cost, the system prioritizes efficient use of limited renewable capacity to displace expensive grid imports.

4.5. Economic Performance: Case 1 vs. Case 2 NPV Analysis

The economic analysis reveals that both configurations deliver substantial positive net present value improvements relative to the grid-only reference case, though with significantly different magnitudes and return profiles.

Case 1 generates a ΔNPV of 9,166,437 € over the 25-year project lifetime, representing a 105.8% return on the initial capital investment of 8,665,465 €. This strong economic performance results from the combination of avoided electricity purchases (reduced OPEX), revenue from grid export sales, and carbon tax avoidance benefits. Annual OPEX for Case 1 totals 285,727 €, representing an 80.2% reduction compared to the reference grid-only OPEX of 1,440,200 €. This operational cost saving of 1,154,473 € per year provides the primary economic value driver.

Annual revenue from grid export reaches 240,458 €, generated from 1384.2 MWh exported at an equivalent cost of 0.17 €/kWh that includes the potential carbon credit benefits. While this represents only a secondary economic contribution compared to avoided imports, it provides a steady cash flow during high-production months and improves project bankability for debt financing.

The simple payback period for Case 1 can be estimated as approximately 6.2 years based on an annual cash flow of approximately 1,395,000 € (OPEX savings plus export revenue). The NPV analysis using a 6% discount rate appropriately accounts for the time value of money, with the cumulative discounted cash flows substantially exceeding initial capital by end-of-life.

Case 2 achieves a ΔNPV of 4,463,027 € despite the capital budget constraint, representing a 223.2% return on the 1,999,849 € investment—significantly higher ROI percentage than Case 1. This superior relative performance reflects the diminishing marginal returns of oversized systems: the first units of PV and storage capacity provide the highest economic value by displacing the most expensive grid imports, while incremental additions yield progressively lower returns.

Annual OPEX for Case 2 totals 950,662 €, a 34.0% reduction versus the grid-only reference. The operational savings of 489,538 € per year are substantially lower than Case 1 due to continued grid dependence (3266.2 MWh import versus 1012.4 MWh in Case 1). Export revenue drops to just 16,031 € annually from minimal 91.1 MWh exports, confirming that the system is sized for self-consumption rather than surplus generation.

The simple payback period for Case 2 is approximately 3.9 years, notably shorter than Case 1 despite lower absolute savings. This faster payback makes the project more attractive for investors with capital constraints or shorter investment horizons. The higher NPV per euro invested (2.23 versus 1.06) demonstrates superior capital efficiency, though at the cost of reduced total economic value and energy autonomy.

The economic comparison reveals a fundamental trade-off: Case 1 maximizes absolute value creation and energy autonomy but requires substantial capital and delivers lower percentage returns, while Case 2 optimizes capital efficiency and achieves faster payback but sacrifices total value and remains grid-dependent. The choice between these strategies

depends on investor priorities, capital availability, risk tolerance, and strategic objectives regarding energy security versus financial optimization.

4.6. Environmental Impact: Case 1 vs. Case 2 Emissions Assessment

Figure 10 presents the carbon emissions analysis under the Scope 2 accounting methodology, quantifying the environmental benefits of renewable energy integration.

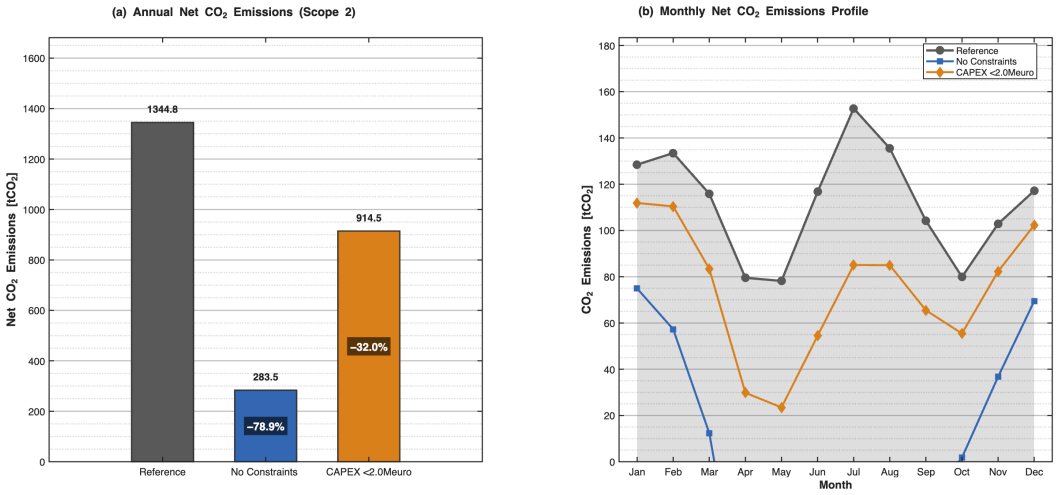

Figure 10. CO_2 emissions comparison: (**a**) annual net emissions for reference and both cases with reduction percentages; (**b**) monthly emissions profile showing seasonal variations.

The reference case (grid-only supply) generates 1344.8 tonnes of CO_2 annually based on 4802.8 MWh demand and 0.280 $kgCO_2/kWh$ grid carbon intensity. This baseline represents the environmental impact of a conventional electricity supply without renewable integration.

Case 1 reduces annual emissions to 283.5 tCO_2, achieving a 78.9% reduction (1061.3 tCO_2 avoided annually). This substantial decarbonization directly correlates with the 78.9% self-sufficiency, as locally generated solar electricity displaces grid imports. Over the 25-year project lifetime, cumulative emissions avoidance reaches 26,533 tCO_2, equivalent to removing approximately 5750 passenger vehicles from roads for one year.

At the assumed carbon price of 100 €/tonne, the annual carbon tax savings total 106,130 €, contributing approximately 7.5% to the total annual economic benefit. While secondary to direct energy cost savings, these carbon benefits become increasingly significant under scenarios of rising carbon prices projected under stringent climate policies. At 150 €/tCO_2 (a plausible 2030 price under EU ETS projections), carbon savings would increase to 159,195 € annually, improving project economics further.

Case 2 achieves 914.5 tCO_2 annual emissions, a 32.0% reduction (430.3 tCO_2 avoided). This more modest decarbonization reflects the lower self-sufficiency and continued grid dependence. Lifetime emissions avoidance totals 10,758 tCO_2, less than half the Case 1 value but still representing meaningful environmental impact. Annual carbon tax savings at 100 €/tonne amount to 43,030 €.

The monthly emissions profile (Figure 10b) reveals pronounced seasonal variations for both renewable configurations. Reference case emissions remain relatively stable around 110–115 tCO_2/month with some variation due to demand seasonality. Case 1 shows relevant monthly fluctuation, ranging from near-zero during summer months (June–August achieve 2–12 tCO_2) to 75 tCO_2 in January. This pattern mirrors the inverse of solar resource availability—winter months with low irradiance require grid import and generate emissions, while summer months achieve near-complete renewable supply.

Case 2 exhibits similar seasonal patterns but with higher baseline emissions due to consistent grid dependence. Monthly values range from 68 tCO_2 in July to 103 tCO_2 in March, never achieving the near-zero levels of Case 1 during optimal months. The reduced amplitude of seasonal variation reflects the system's limited capacity to fully satisfy even summer demand through solar generation.

The emissions analysis demonstrates that energy autonomy and carbon reduction are strongly coupled objectives—configurations optimized for economic performance simultaneously deliver environmental benefits proportional to renewable energy penetration. This alignment suggests that carbon pricing mechanisms effectively internalize environmental externalities, creating economic incentives that support climate objectives.

4.7. System Operational Characteristics: Case 1 vs. Case 2 Grid Interaction

Detailed examination of the operational profiles reveals distinct grid interaction patterns between the two configurations. Case 1 exhibits highly dynamic bidirectional grid exchange, with frequent transitions between import and export states depending on solar availability and battery state-of-charge. Peak export events reach the 1000 kW grid connection limit during midday high-irradiance periods in summer, suggesting that the oversized PV capacity occasionally experiences curtailment or requires grid reinforcement for full utilization.

Import events in Case 1 occur primarily during nighttime hours when solar generation is unavailable, and battery discharge is either insufficient or depleted after multi-day low-irradiance periods. The large battery capacity (12.3 MWh) enables extended energy storage, with state-of-charge cycles spanning multiple days during summer months. Winter operation shows daily cycling patterns with partial discharge depths, as limited solar charging prevents full battery utilization.

Case 2 demonstrates more consistent import-dominant grid interaction with minimal export activity. The smaller battery (1.68 MWh) operates on daily charging cycles, typically reaching full charge around midday during high-irradiance periods and discharging to minimum SOC overnight. This regular cycling pattern maximizes battery utilization factor but provides limited multi-day buffering capability against weather variability.

The grid connection utilization analysis shows that Case 1 uses the full 1000 kW bidirectional capacity, occasionally reaching limits during peak import and export events, while Case 2 rarely exceeds 1000 kW in either direction. This suggests that the budget-constrained configuration could potentially operate with reduced grid connection capacity, offering additional capital savings through downsized transformer and switchgear requirements.

4.8. CAPEX Sensitivity Analysis

The three-dimensional sensitivity analysis spanning 48 scenarios reveals complex interdependencies among technology costs, carbon intensity, and optimal system configurations. To present the results clearly, the authors report the cost-sensitivity surfaces at a fixed reference value of $f_{CO_2} = 0.280$ $kgCO_2/kWh$, consistent with the constant-emission-factor assumption stated in Section 3.3. This slicing of the full 3D sweep isolates PV and battery CAPEX effects while maintaining the same computational framework for the other carbon-intensity levels.

Figure 11 presents six contour maps characterizing the optimal design space as functions of PV and battery specific costs. These visualizations employ a consistent two-dimensional parameter space representation with PV costs on the horizontal axis (400–1200 €/kW_p) and battery costs on the vertical axis (400–1000 €/kWh). The contour patterns, level spacing, and color gradients collectively reveal fundamental economic and technical relationships governing system design.

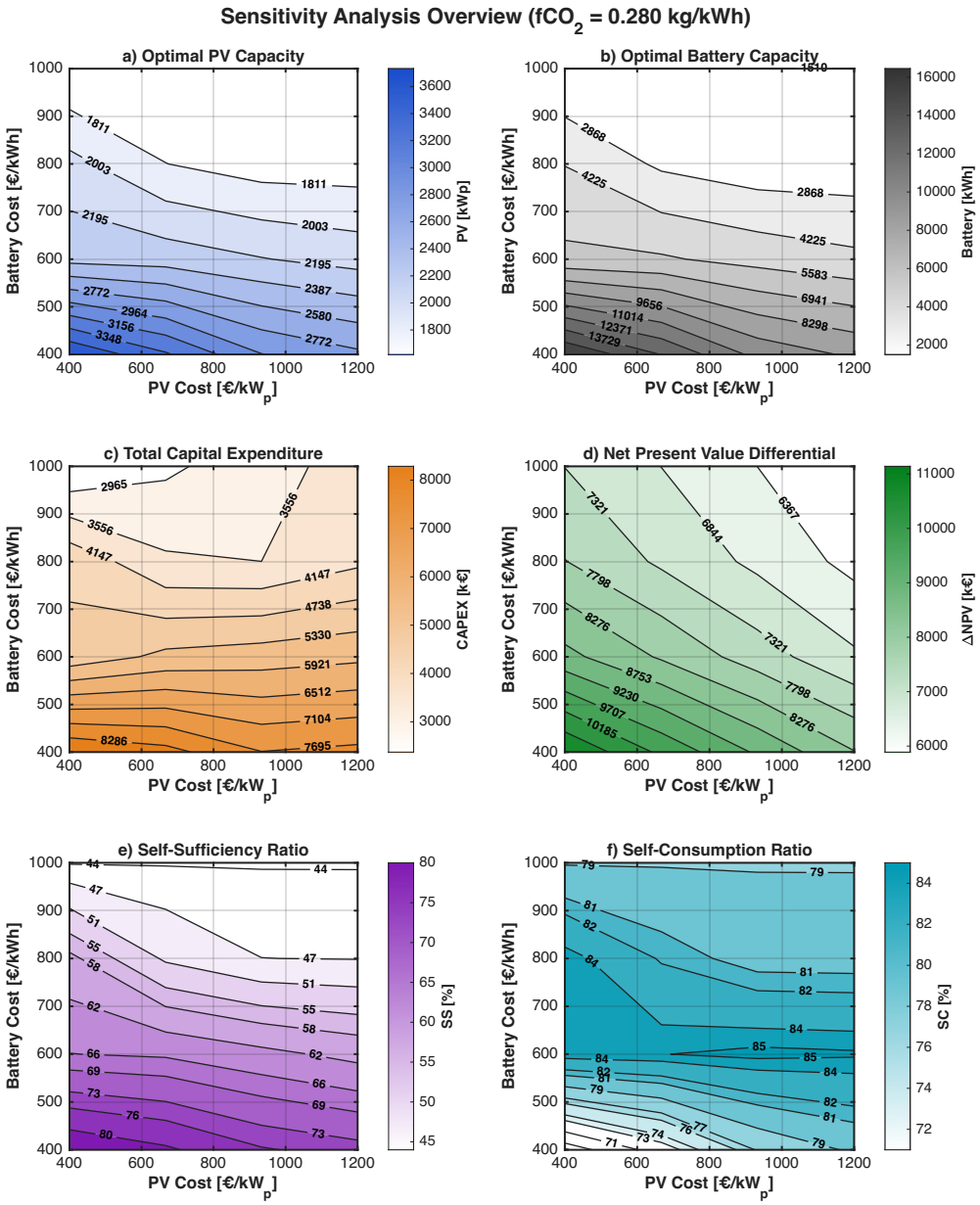

Figure 11. Contour maps showing optimal system configurations and performance metrics as functions of PV- and battery-specific costs under moderate carbon intensity (0.280 $kgCO_2$/kWh). Top row: (**a**) optimal PV capacity increases with decreasing PV costs and shows modest sensitivity to battery costs; (**b**) optimal battery capacity exhibits strong inverse relationship with battery costs and increases with lower PV costs. Middle row: (**c**) total CAPEX reflects combined investment in both technologies; (**d**) NPV differential reaches maximum at lowest cost combination while transitioning through zero at critical cost thresholds. Bottom row: (**e**) self-sufficiency increases strongly with both PV and battery capacity, requiring coordination of both technologies; (**f**) self-consumption exhibits strong dependence on system sizing with peak values achieved when battery storage balances generation and consumption patterns.

4.8.1. Optimal PV Capacity: Cost Sensitivity and Break-Even Thresholds

Panel (a) of Figure 11 shows that optimal PV capacity remains primarily driven by PV-specific costs, while battery costs influence PV sizing through storage-enabled self-consumption. The predominantly vertical orientation of iso-capacity contours indicates that PV investment decisions respond strongly to PV cost variations, with secondary modulation by storage cost.

At the lowest PV cost (400 €/kW$_p$) and low battery cost (400 €/kWh), the optimization selects large PV capacities around 3.7 MW$_p$, corresponding to approximately 6.3 GWh annual PV generation. As battery costs rise to 1000 €/kWh at the same PV cost, optimal PV capacity contracts to about 1.6 MW$_p$, with annual PV generation near 2.7 GWh.

Across the explored PV cost range (400–1200 €/kW$_p$), PV capacity declines monotonically and converges toward the lower bound at high costs. For example, at $C_{PV} = 1200$ €/kW$_p$ the optimal PV capacity spans roughly 1.6–2.8 MW$_p$ depending on storage cost, indicating that higher PV CAPEX materially compresses deployment even when carbon intensity is fixed.

Battery cost still shapes PV sizing by altering the value of self-consumption: at $C_{PV} = 400$ €/kW$_p$, PV capacity ranges from about 1.6 to 3.7 MW$_p$ as C_{batt} varies from 1000 to 400 €/kWh. This interaction weakens at higher PV costs, where optimal PV capacities cluster near the lower bound.

4.8.2. Optimal Battery Capacity: Derived Value and Synergies

Panel (b) presents a markedly different sensitivity pattern for battery capacity, with diagonally oriented contours indicating coupled dependence on both PV and battery costs. This two-dimensional sensitivity reflects the derived nature of battery value: storage becomes economically attractive only when substantial PV generation creates temporal arbitrage opportunities. The fundamental asymmetry between PV and battery economics is clearly visible: PV contours are predominantly vertical (PV-cost driven), whereas battery contours are diagonal (jointly determined by both costs).

Maximum battery capacities reach approximately 16.4 MWh in the low-cost corner ($C_{PV} = 400$ €/kW$_p$, $C_{batt} = 400$ €/kWh), while even at $C_{PV} = 1200$ €/kW$_p$ and $C_{batt} = 400$ €/kWh, the optimal battery size remains near 9.4 MWh. These large sizes arise because low-cost storage can capture substantial midday PV surplus and shift it to evening peaks.

As battery costs increase, optimal storage contracts sharply: at $C_{batt} = 800$ €/kWh, the battery capacity ranges from about 2.0 to 4.2 MWh depending on PV cost, and at $C_{batt} = 1000$ €/kWh, it collapses to approximately 1.5 MWh across all PV cost levels. This behavior reflects the short economic lifetime of batteries under daily cycling and the need to recover CAPEX through limited arbitrage value.

The diagonal contour pattern reveals compensatory relationships: at $C_{batt} = 800$ €/kWh, lowering PV cost from 1200 to 400 €/kW$_p$ increases the optimal battery capacity from about 2.0 to 4.2 MWh; at $C_{batt} = 600$ €/kWh, the corresponding increase is roughly 4.5 to 5.9 MWh. This confirms that cheaper PV amplifies the economic value of storage by increasing surplus energy available for shifting.

Conversely, at the highest battery costs the solution converges toward the minimum storage level, indicating that storage becomes marginal under the assumed tariff structure and carbon intensity when CAPEX is high.

4.8.3. CAPEX Sensitivity to KPIs

Looking at the other KPIs related to overall CAPEX, NPV, SS and SC, the authors have presented some practical considerations below.

Investment and profitability The total capital expenditure varies from ∼2.37 M€ (about 2373 k€) up to ∼8.88 M€ (about 8878 k€). Notably, the highest total CAPEX is reached in the low-unit-cost corner, where the optimizer exploits cheaper technologies by scaling up both PV and storage, thereby increasing absolute investment despite lower specific costs. Conversely, in the high-C_{batt} region, the design shifts toward a "minimal-storage" regime (battery capacity collapses), and total CAPEX becomes more visibly influenced by

C_{PV}, producing the observed change in contour orientation (i.e., a clearer increase in total CAPEX as PV becomes more expensive).

The net present value differential ΔNPV decreases smoothly from ∼11.14 M€ (about 11,139 k€) down to ∼5.89 M€ (about 5889 k€) as either technology becomes more expensive. The near-diagonal iso-ΔNPV contours indicate that PV and battery costs act as partially substitutable levers from an economic standpoint: increases in one component CAPEX can be partially offset by reductions in the other, because both contribute to the same underlying value stream (reducing grid purchases and reshaping import/export profiles).

Self-Sufficiency and Self-Consumption The self-sufficiency (SS) increases strongly as costs decrease, moving from ∼44% in the high-cost region to up to ∼84% in the low-cost corner. The gradient of the SS surface is steeper along the battery-cost axis, confirming that storage cost is the primary driver for achieving high autonomy at fixed f_{CO_2}: inexpensive storage allows PV energy to be shifted to non-solar hours, thereby reducing reliance on the grid and raising the fraction of demand met locally.

In contrast, the self-consumption (SC) shows a distinctly non-monotonic behavior and spans a narrower range (approximately 68–85%). In the low-cost corner, SC drops to the lowest values (around 68–77%) even though SS is the highest. This apparent counter-trend is consistent with PV oversizing: when PV (and storage) are cheap, the optimizer can install larger PV capacities to maximize absolute value, but a larger PV fleet also produces more surplus generation relative to instantaneous demand, which reduces the fraction of PV generation that is consumed on-site. As PV and/or battery costs increase, the system is progressively "right-sized" (less surplus), and SC rises toward ∼84–85% for intermediate cost combinations. In the high-C_{batt} region, SC settles around ∼79–82%, reflecting limited shifting capability and a PV size that is constrained primarily by direct self-consumption.

Taken together, the bottom-row indicators emphasize a key design insight at $f_{CO_2} = 0.280$ kgCO_2/kWh: lowering CAPEX mainly pushes the solution toward higher autonomy (SS) through larger PV+storage installations, but it can simultaneously reduce PV utilization efficiency (SC) due to increased surplus generation. This highlights a fundamental trade-off between maximizing local supply coverage and maximizing the fraction of PV generation absorbed on-site, which becomes especially visible in the low-cost regime.

4.8.4. Impact of Other Parameters to Sensitivity Analysis

Beyond CAPEX, outcomes depend on tariff asymmetry, discounting, and carbon valuation. In the base case, the export tariff is set to half of the import price (2:1 ratio), with a 6% discount rate and a 100 €/tCO_2 carbon price; narrower export discounts or lower discount rates tend to support larger systems, whereas tighter export remuneration or higher discount rates shift the optimum toward smaller, faster-payback configurations. Higher carbon prices strengthen the economic case for larger renewable shares. Demand response and load variability are not modeled here, but can be incorporated through flexible-load variables and stochastic or sectoral load profiles.

4.9. Discussion and Limitations

The results demonstrate that the integrated MILP framework effectively captures the interplay between investment constraints and operational performance, providing actionable design guidance for energy community planners. Several interpretive remarks and scope caveats merit discussion.

Financial trade-offs. The comparison between Case 1 (unconstrained) and Case 2 (budget-constrained) reveals a clear diminishing-returns effect: Case 2 delivers superior capital efficiency (223% return on investment, 3.9-year payback) despite lower absolute performance, because the optimizer preferentially allocates limited capital to PV rather

than storage, where the first kWp provides higher marginal value than incremental kWh of battery. This suggests that modular deployment—starting with a right-sized, fast-payback configuration and scaling up as capital or incentives evolve—is a financially robust strategy.

Policy sensitivity. The jointly optimized planning–dispatch model is highly sensitive to the electricity price ratio (purchase:export = 2:1 in this study). Such asymmetry incentivizes self-consumption and penalizes surplus exports, shaping MILP-derived optimal capacities. Adjusted tariff structures—such as time-differentiated export remuneration or expanded net-metering—could encourage configurations with broader system benefits. The analysis confirms that financially optimal solutions under realistic price and carbon signals inherently support decarbonization: configurations maximizing NPV also achieve CO_2 reductions closely proportional to renewable penetration, reinforcing the role of carbon pricing as a mechanism aligning private investment with societal climate goals.

Scope limitations. As detailed in Section 2, the model does not include explicit battery or PV degradation, mid-life component replacement, O&M costs, or distribution network constraints. The electricity price profile follows a time-of-use structure with hourly differentiation (0.25–0.30 €/kWh), but the same annual tariff is repeated over 25 years without escalation; future tariff evolution and real-time pricing could shift optimal configurations. These simplifications are appropriate for a master-planning study aimed at identifying cost-driven design thresholds, but should be relaxed in detailed project-level analyses. The extensions identified here are addressed in the future work outlined below.

5. Conclusions

This study developed and applied an integrated MILP-based techno-economic optimization framework for sizing photovoltaic (PV) and battery energy storage systems (BESSs) in a grid-connected educational energy community, co-optimizing design variables and hourly dispatch over a 25-year horizon within a single mathematical program. The core methodological contribution—solving investment sizing and operational scheduling concurrently—avoids the sequential decoupling typical of conventional planning workflows and ensures full consistency among capacity decisions, temporal variability of renewable generation, storage dynamics, and time-varying tariff signals.

The comparative analysis of two design scenarios yields the following principal findings:

- **Case 1 (unconstrained):** The economically optimal configuration installs 3194 kWp PV and 12,312 kWh battery storage, requiring 8.67 M€ CAPEX and delivering a differential NPV of 9.17 M€ over 25 years. This system achieves 78.9% self-sufficiency, 74.3% self-consumption, and a 78.9% reduction in Scope 2 CO_2 emissions (1061 tCO_2/year avoided), with a payback period of 6.2 years.
- **Case 2 (CAPEX $\leq$ 2.0 M€):**The budget-constrained optimum installs 994 kWp PV and 1681 kWh storage, achieving 32.0% self-sufficiency and 94.6% self-consumption with a 4.46 M€ NPV and 3.9-year payback. Despite lower absolute performance, this configuration demonstrates markedly superior capital efficiency (223% return on investment vs. 106%), highlighting the diminishing marginal returns of system oversizing.
- **Technology dominance:** Under current Italian cost and tariff conditions, PV-dominated configurations deliver the highest economic value. Battery storage adds limited benefit unless generous capital budgets or elevated carbon prices are assumed, because the optimizer preferentially allocates constrained capital to PV generation—where the first kWp yields the highest marginal value—rather than to incremental storage.

- **CAPEX sensitivity:** A systematic 48-scenario sensitivity analysis maps break-even regions across PV and battery cost ranges. PV cost emerges as the primary lever governing optimal capacity and NPV, while battery cost modulates storage adoption through its effect on self-consumption value. The resulting contour surfaces provide actionable technology-cost thresholds for investment planning.

From a financial and strategic perspective, the results reveal a clear trade-off between energy autonomy and capital efficiency: Case 1 maximizes absolute value creation and emissions reduction but requires substantial capital and longer payback, whereas Case 2 optimizes capital productivity with faster returns at the cost of continued grid dependence. Modular deployment—starting with a right-sized, fast-payback configuration and scaling up as technology costs decline or incentive frameworks evolve—emerges as a financially robust and operationally consistent strategy.

The analysis also confirms that the jointly optimized planning–dispatch model is highly sensitive to regulatory parameters, particularly the purchase-to-export price ratio (2:1 in this study). Configurations that maximize NPV simultaneously achieve CO_2 reductions closely proportional to renewable penetration, reinforcing the role of carbon pricing as a robust policy mechanism aligning private investment decisions with societal climate goals. As renewable energy communities gain regulatory recognition across the European Union, the framework offers planners and policymakers a computationally efficient tool to evaluate site-specific design options under diverse financial and environmental constraints.

Future work will extend the framework along the following directions: (i) incorporation of battery degradation models (calendar and cycle aging) via piecewise-linear state-of-health constraints and PV annual degradation to capture long-term performance decay [37,38]; (ii) mid-life battery and inverter replacement scheduling with discounted replacement cost terms; (iii) explicit modeling of tariff evolution, carbon price uncertainty, and stochastic or robust optimization extensions to assess long-term investment robustness; (iv) demand–response integration and sector-specific load decomposition (heating, cooling, mobility) to explore flexible-load synergies; and (v) distribution network constraints (voltage, congestion, hosting capacity) to account for grid-integration limitations. As technology costs continue their decline and regulatory frameworks increasingly support distributed resources, periodic reassessment using the modular MILP platform will support informed, site-specific investment decisions in the transition toward decarbonized energy communities.

Author Contributions: Conceptualization, S.M. and B.N.; methodology, S.M.; software, S.M.; validation, S.M., B.N. and M.M.; formal analysis, S.M.; investigation, S.M.; resources, S.M. and K.Y.; data curation, S.M.; writing—original draft preparation, S.M.; writing—review and editing, S.M., B.N., K.Y. and M.M.; visualization, S.M.; supervision, B.N. and M.M.; project administration, S.M. All authors have read and agreed to the published version of the manuscript.

Funding: This work was supported by the Italian Ministry of University and Research (MUR) under the European Union Next Generation EU program (PNRR—M4C2—ECS_00000024 "Rome Technopole", Flagship Project 2: "Energy transition and digital transition in urban regeneration and construction").

Institutional Review Board Statement: Not applicable.

Informed Consent Statement: Not applicable.

Data Availability Statement: The data presented in this study are available on request from the corresponding author. The data are not publicly available due to proprietary constraints related to the energy community's operational and contractual agreements.

Conflicts of Interest: The authors declare no conflicts of interest.

Nomenclature

Symbols

$\mathcal{T}$	Set of hourly time steps ($\lvert\mathcal{T}\rvert = 8760$)
t	Time-step index
Δt	Time-step duration (h)
$P_{\text{load},t}$	Electrical load at time t (kW)
$P_{\text{el,base},t}$	Base electrical demand at time t (kW)
$\dot{Q}_{\text{cool},t}$	Cooling thermal power demand at time t (kW_{th})
$\dot{Q}_{\text{heat},t}$	Heating thermal power demand at time t (kW_{th})
COP_{cool}	Coefficient of performance of the cooling system (-)
η_{heat}	Heating system efficiency (-)
$P_{\text{DR},t}$	Demand–response load reduction at time t (kW)
n_{PV}	Number of PV modules (-)
P_t^{PV}	PV AC power output at time t (kW)
$G_{\text{POA},t}$	Plane-of-array irradiance at time t (W/m^2)
G_{STC}	Standard test condition irradiance (W/m^2)
S_{unit}	PV module surface area (m^2)
$\eta_{\text{PV}}(\cdot)$	PV conversion efficiency (-)
η_{bos}	Balance-of-system efficiency (-)
$E_{\text{batt,size}}$	Nominal battery energy capacity (kWh)
E_t	Battery state of charge at time t (kWh)
P_t^{ch}	Battery charging power at time t (kW)
P_t^{dch}	Battery discharging power at time t (kW)
$\eta_{\text{ch}}, \eta_{\text{dch}}$	Battery charge and discharge efficiencies (-)
$P_{g,t}^{+}, P_{g,t}^{-}$	Grid import and export power at time t (kW)
p_t^{+}, p_t^{-}	Electricity import and export prices at time t (€/kWh)
ΔNPV	Differential net present value (EUR)
f_{CO_2}	Grid emission factor ($\text{kgCO}_2\text{/kWh}$)

Acronyms

BESS	Battery energy storage system
CAPEX	Capital expenditure
COP	Coefficient of performance
DNI	Direct normal irradiance
DR	Demand response
LCOE	Levelized cost of electricity
LCOS	Levelized cost of storage
MILP	Mixed-integer linear programming
NPV	Net present value
POA	Plane of array
PV	Photovoltaic
SoC	State of charge
STC	Standard test conditions
VRE	Variable renewable energy

References

1. IEA PVPS. Task 1. In *Trends in Photovoltaic Applications 2024*; International Energy Agency PVPS: Paris, France, 2024; ISBN 978-3-907281-68-0.
2. IEA PVPS. *Snapshot of Global PV Markets 2025*; International Energy Agency PVPS: Paris, France, 2025.
3. Philipps, S.; Warmuth, W. *Photovoltaics Report*; Fraunhofer ISE: Freiburg im Breisgau, Germany, 2025. Available online: https://www.ise.fraunhofer.de/en/publications/studies/photovoltaics-report.html (accessed on 1 February 2026).
4. IRENA. *Renewable Power Generation Costs in 2023*; IRENA: Abu Dhabi, United Arab Emirates, 2024.
5. Lazard. *Levelized Cost of Energy+ (LCOE+)*; Lazard LLC: New York, NY, USA, June 2025. Available online: https://www.lazard.com/research-insights/levelized-cost-of-energyplus-lcoeplus/ (accessed on 1 February 2026).

6. Rubin, E.S.; Azevedo, I.M.; Jaramillo, P.; Yeh, S. A review of learning rates for electricity supply technologies. *Energy Policy* **2015**, *86*, 198–218. [CrossRef]
7. Nagy, B.; Farmer, J.D.; Bui, Q.M.; Trancik, J.E. Statistical basis for predicting technological progress. *PLoS ONE* **2013**, *8*, e52669.
8. Blair, N.; Augustine, C.; Cole, W.; Denholm, P.; Frazier, W.; Geocaris, M.; Jorgenson, J.; McCabe, K.; Podkaminer, K.; Prasanna, A.; et al. *Storage Futures Study: Key Learnings for the Coming Decades*; NREL/TP-7A40-81779; National Renewable Energy Laboratory: Golden, CO, USA, 2022.
9. Denholm, P.; Jorgenson, J.; Hummon, M.; Jenkin, T.; Palchak, D.; Kirby, B.; Ma, O.; O'Malley, M. *The Value of Energy Storage for Grid Applications*; NREL/TP-6A20-58465; National Renewable Energy Laboratory: Golden, CO, USA, 2013.
10. Schmidt, O.; Melchior, S.; Hawkes, A.; Staffell, I. Projecting the Future Levelized Cost of Electricity Storage Technologies. *Joule* **2019**, *3*, 81–100. [CrossRef]
11. Cole, W.; Frazier, A.W. *Cost Projections for Utility-Scale Battery Storage*; NREL/TP-6A20-73222; National Renewable Energy Laboratory: Golden, CO, USA, 2019.
12. Denholm, P.; Cole, W.; Blair, N. *Moving Beyond 4-Hour Li-Ion Batteries: Challenges and Opportunities for Long(er)-Duration Energy Storage*; NREL/TP-6A40-85878; National Renewable Energy Laboratory: Golden, CO, USA, 2023.
13. Luthander, R.; Widén, J.; Nilsson, D.; Palm, J. Photovoltaic self-consumption in buildings: A review. *Appl. Energy* **2015**, *142*, 80–94. [CrossRef]
14. European Union. *Directive (EU) 2019/944 on Common Rules for the Internal Market for Electricity*; European Union: Brussels, Belgium, 2019.
15. World Bank. *State and Trends of Carbon Pricing 2024*; World Bank: Washington, DC, USA, 2024.
16. High-Level Commission on Carbon Prices. *Report of the High-Level Commission on Carbon Prices*; World Bank: Washington, DC, USA, 2017.
17. Stadler, M.; Groissböck, M.; Cardoso, G.; Marnay, C. Optimizing Distributed Energy Resources and building retrofits with the strategic DER-CAModel. *Appl. Energy* **2014**, *132*, 557–567. [CrossRef]
18. Mashayekh, S.; Stadler, M.; Cardoso, G.; Heleno, M. A mixed integer linear programming approach for optimal DER portfolio, sizing, and placement in multi-energy microgrids. *Appl. Energy* **2017**, *187*, 154–168. [CrossRef]
19. DiOrio, N.; Dobos, A.; Janzou, S.; Nelson, A.; Lundstrom, B. *Technoeconomic Modeling of Battery Energy Storage in SAM*; NREL/TP-6A20-64641; National Renewable Energy Laboratory: Golden, CO, USA, 2015.
20. Terlouw, T.; AlSkaif, T.; Bauer, C.; van Sark, W. Multi-objective optimization of energy arbitrage in community energy storage systems using different battery technologies. *Appl. Energy* **2019**, *239*, 356–372. [CrossRef]
21. Das, M.; Singh, M.A.K.; Biswas, A. Techno-economic optimization of an off-grid hybrid renewable energy system using metaheuristic optimization approaches–Case of a radio transmitter station in India. *Energy Convers. Manag.* **2019**, *185*, 339–352. [CrossRef]
22. Zhao, X.; Zhang, Z.; Xie, Y.; Meng, J. Economic-environmental dispatch of microgrid based on improved quantum particle swarm optimization. *Energy* **2020**, *195*, 117014. [CrossRef]
23. Li, Y.; Peng, J.; Jia, H.; Zou, B.; Hao, B.; Ma, T.; Wang, X. Optimal battery schedule for grid-connected photovoltaic-battery systems of office buildings based on a dynamic programming algorithm. *J. Energy Storage* **2022**, *50*, 104557. [CrossRef]
24. Ziegler, M.S.; Mueller, J.M.; Pereira, G.D.; Song, J.; Ferrara, M.; Chiang, Y.M.; Trancik, J.E. Storage Requirements and Costs of Shaping Renewable Energy Toward Grid Decarbonization. *Joule* **2019**, *3*, 2134–2153. [PubMed]
25. King, D.L.; Boyson, W.E.; Kratochvil, J.A. *Photovoltaic Array Performance Model*; SAND2004-3535; Sandia National Laboratories: Albuquerque, NM, USA, 2004.
26. Faiman, D. Assessing the outdoor operating temperature of PV modules. *Prog. Photovolt. Res. Appl.* **2008**, *16*, 307–315. [CrossRef]
27. Anderson, K.; Kemnitz, J.; Boyd, M. Evaluating cell temperature models and the effect of wind speed in PV system capacity testing. In *2021 IEEE 48th Photovoltaic Specialists Conference (PVSC)*; IEEE: Piscataway, NJ, USA, 2021; Volume 2, pp. 1663–1669. [CrossRef]
28. Dal Cin, E.; Carraro, G.; Volpato, G.; Lazzaretto, A.; Danieli, P. A multi-criteria approach to optimize the design-operation of Energy Communities considering economic-environmental objectives and demand side management. *Energy Convers. Manag.* **2022**, *263*, 115677. [CrossRef]
29. Carraro, G.; Dal Cin, E.; Rech, S. Integrating Energy Generation and Demand in the Design and Operation Optimization of Energy Communities. *Energies* **2024**, *17*, 6358. [CrossRef]
30. Fan, G.; Liu, Z.; Liu, X.; Shi, Y.; Wu, D.; Guo, J.; Zhang, S.; Yang, X.; Zhang, Y. Energy management strategies and multi-objective optimization of a near-zero energy community energy supply system combined with hybrid energy storage. *Sustain. Cities Soc.* **2022**, *83*, 103970. [CrossRef]
31. Zatti, M.; Moncecchi, M.; Gabba, M.; Chiesa, A.; Bovera, F.; Merlo, M. Energy Communities Design Optimization in the Italian Framework. *Appl. Sci.* **2021**, *11*, 5218. [CrossRef]

32. Talluri, G.; Lozito, G.M.; Grasso, F.; Iturrino Garcia, C.; Luchetta, A. Optimal Battery Energy Storage System Scheduling within Renewable Energy Communities. *Energies* **2021**, *14*, 8480. [CrossRef]
33. Simoiu, M.S.; Fagarasan, I.; Ploix, S.; Calofir, V. Sizing and Management of an Energy System for a Metropolitan Station with Storage and Related District Energy Community. *Energies* **2021**, *14*, 5997. [CrossRef]
34. Ciocia, A.; Amato, A.; Di Leo, P.; Fichera, S.; Malgaroli, G.; Spertino, F.; Tzanova, S. Self-Consumption and Self-Sufficiency in Photovoltaic Systems: Effect of Grid Limitation and Storage Installation. *Energies* **2021**, *14*, 1591. [CrossRef]
35. Terrier, C.; Loustau, J.R.H.; Lepour, D.; Marechal, F. From Local Energy Communities towards National Energy System: A Grid-Aware Techno-Economic Analysis. *Energies* **2024**, *17*, 910. [CrossRef]
36. De Souza, R.J.; Reini, M.; Serra, L.M.; Lozano, M.A.; Nadalon, E.; Casisi, M. Multi-Objective Optimization of an Energy Community Powered by a Distributed Polygeneration System. *Energies* **2024**, *17*, 3085. [CrossRef]
37. Edge, J.S.; O'Kane, S.; Prosser, R.; Kirkaldy, N.D.; Patel, A.N.; Hales, A.; Ghosh, A.; Ai, W.; Chen, J.; Yang, J.; et al. Lithium-ion battery degradation: What you need to know. *Phys. Chem. Chem. Phys.* **2021**, *23*, 8200–8221. [CrossRef]
38. Naumann, M.; Schimpe, M.; Keil, P.; Hesse, H.C.; Jossen, A. Analysis and modeling of calendar aging of a $LiFePO_4$/graphite cell. *J. Energy Storage* **2018**, *17*, 153–169. [CrossRef]
39. Löfberg, J. YALMIP: A toolbox for modeling and optimization in MATLAB. In *2004 IEEE International Conference on Robotics and Automation*, Taipei, Taiwan, 2–4 September 2004; IEEE: Piscataway, NJ, USA, 2004.
40. Gurobi Optimization, LLC. *Gurobi Optimizer Reference Manual*, Version 12; Gurobi Optimization: Houston, TX, USA, 2025.